An analytical formulation for turbulent kinetic energy added by wind turbines based on large-eddy simulation

Ali Khanjari[1], Asim Feroz[1], and Cristina Archer[1]

[1]Center for Research in Wind (CReW), University of Delaware, 221 Academy St, Newark, DE 19716, USA

Correspondence: Cristina Archer (carcher@udel.edu)

Abstract. Wind turbine wakes are plume-like regions characterized by reduced wind speed and enhanced turbulent kinetic energy (TKE) that form downstream of wind turbines. Numerical mesoscale models, like the Weather Research and Forecast (WRF) model, are generally effective at reproducing the wind speed deficit, but lack skills at simulating the TKE added by wind turbines. Here we propose an analytical formulation for added TKE by a wind turbine that reproduces, via least-square error parameter fitting, the main features of the three-dimensional structure of added TKE as simulated in previous large-eddy simulation (LES) studies, including: a streamwise peak at x = 4D–6D (where D is the turbine diameter), a vertical peak near the upper rotor region, and an annular Gaussian-like distribution along the rotor edge. Validation of the proposed formulation against independent LES results and wind tunnel observations from the literature indicates a promising performance in the case of a single wind turbine wake. The ultimate goal is to insert the proposed formulation, after further improvements, in the WRF model for use within existing or new wind farm parameterizations.

1 Introduction

Over the last two decades, there has been a significant surge in renewable energy, especially wind energy, due to its vast potential worldwide (Archer and Jacobson, 2005) and to the global shift towards low- or no-carbon sources of energy to fight global climate change. For the first time in history wind has provided over 10% of the total electricity production of the world, with a global total installed capacity of approximately 824 GW (International Renewable Energy Agency (IRENA), 2022).

When wind turbines are installed in a wind farm, their layout is a compromise between two opposite needs. On one hand, the distance between turbines should be as small as possible to minimize the total lease area and to reduce cable length costs. On the other hand, their distance should be as large as possible to minimize so-called "wake losses" and maximize total power output. Wake losses are the undesirable consequence of wakes, which are plume-like regions characterized by reduced wind speed and enhanced turbulent kinetic energy (TKE) that form downstream of wind turbines (Stevens and Meneveau, 2017). As a result of the reduced wind speed and the enhanced turbulence in the wakes, not only is the performance of downstream turbines in the same wind farm reduced (Archer et al., 2018), but so is also the power production of neighbouring wind farms (Nygaard, 2014). As such, wake losses are one of the most important issues affecting wind farm production today (Göçmen et al., 2016) and the correct estimation and prediction of wind turbine wakes and their evolution are fundamental to ultimately ensure reliable power production from a wind farm (Ye et al., 2023).

Historically, most analytical wake models were developed to address the issue of wake impacts on power production of downstream turbines, thus they focused on the most relevant parameter, the wind speed deficit; only a few were developed to address the issue of added turbulence (discussed later). Jensen (1983) proposed the first analytical wake model to predict wind speed deficit behind a wind turbine, based on conservation of momentum. The Jensen model predicts a uniform top-hat wind speed deficit across an expanding rotor area that grows with downstream distance x at a specified constant rate. Since then, a series of analytical wake models were proposed with different assumptions (Katic et al., 1986; Larsen, 1988; Frandsen et al., 2006), including that by Barthelmie et al. (2004), who fitted field data with an analytical formula for the hub-height wind speed deficit as an inverse power function of x. The first Gaussian model for the wind speed deficit was developed by Bastankhah and Porté-Agel (2014) and later improved by Xie and Archer (2015), who proposed two different expansion rates along z and y, rather than one for both as in Bastankhah and Porté-Agel (2014), the values of which were found by fitting high-fidelity simulation results. The Gaussian model was also the foundation of more recent formulations (Gao et al., 2016; Wang et al., 2023). A review of the performance of analytical wake loss models for wind speed deficit caused by wind turbines can be found in Archer et al. (2018).

Only a few analytical wake models provide estimates of the added turbulence by wind turbines and they all use turbulence intensity (TI) as the variable of interest. Quarton and Ainslie (1990) suggested the first empirical formulation for the maximum added turbulence intensity by a wind turbine (ΔTI_{max}) by considering the effect of freestream turbulence intensity (TI_∞) and the thrust coefficient of the wind turbine (C_T):

$$\Delta TI_{max} = 4.8 C_T^{0.7} TI_\infty^{0.68} \left(\frac{x}{x_N}\right)^{-0.57}, \tag{1}$$

where x_N is a scaling parameter that represents the length of the near wake. Several modifications to this formulation have been proposed in the literature, for example by Hassan (1993) and Xie and Archer (2015).

One of the most successful variations of Eq. 1 was that introduced by Crespo and Hernández (1996), who divided the wake into two different regions: the near-wake ($x < 3D$, where D is the rotor diameter) and the far-wake ($x \geq 3D$); they then developed a different equation for each:

$$\Delta TI_{max} = \begin{cases} 0.362(1-\sqrt{1-C_T}) & x < 3D \\ 0.73\left(\dfrac{1-\sqrt{1-C_T}}{2}\right)^{0.8325} (TI_\infty)^{-0.0325} \left(\dfrac{x}{D}\right)^{-0.32} & x \geq 3D. \end{cases} \tag{2}$$

The reason for the two different formulations in the two regions is that, in the near-wake, the influence of the rotor aerodynamics, such as blade aerodynamics, stalled flow, and the presence of tip vortices, are predominant on the wake (Vermeer et al., 2003). Tip vortices originate from the blade tips and roots, propagating downstream in helical trajectories over a short distance (Sherry et al., 2013). If the inclination angle is minimal, these tip vortices will be interpreted as cylindrical shear layers (Crespo et al., 1999). These layers expand within the wake due to turbulent diffusion, forming a ring-shaped region characterized by high turbulence intensity and substantial velocity gradients. However, the tip vortices will break down because of instability within a short distance downstream. In the far-wake region, the rotor effects are less important. The wake is fully developed, turbulent diffusion of momentum becomes dominant, and an increased level of turbulence is found, fueled by shear production.

It is generally assumed that velocity and turbulence intensity should remain self-similar and axi-symmetric in the absence of ambient wind shear (Johansson et al., 2003; Xie and Archer, 2015; Cafiero et al., 2020; van der Laan et al., 2023).

The study by Ishihara and Qian (2018) hereafter referred to as IQ2018, is the first in the literature to provide a three-dimensional analytical equation for the turbulence intensity added by a wind turbine in the downstream wake. Their empirical formula contains a Gaussian function in the radial direction r (from the center of the rotor) multiplied by an amplitude function (an inverse function of x) as follows:

$$\Delta TI(x,y,z) = \frac{1}{d + e\frac{x}{D} + f\left(1+\frac{x}{D}\right)^{-2}} \times \left\{ k_1 \exp\left[-\frac{\left(r-\frac{D}{2}\right)^2}{2\sigma^2} \right] + k_2 \exp\left[-\frac{\left(r+\frac{D}{2}\right)^2}{2\sigma^2} \right] \right\} - \delta(z) \tag{3}$$

$$\delta(z) = \begin{cases} 0 & z \geq H \\ TI_\infty \sin\left(\pi \dfrac{H-z}{H}\right)^2 & z < H, \end{cases} \tag{4}$$

where H is the turbine hub height, d, e, f, k_1, k_2, and σ are functions of C_T and TI_∞ of the form $aC_T^b TI_\infty^c$. We note that also Eq. 1 can be reduced to this same form and Eq. 2 to a close form (with $(1-\sqrt{1-C_T})^b$ instead of C_T^b).

Li et al. (2022) later hypothesized that the added turbulence intensity ΔTI in the streamwise direction has a similar self-similarity property as the velocity deficit and proposed a three-dimensional analytical formula for added turbulence intensity similar to that by Ishihara and Qian (2018). Tian et al. (2022) developed a three-dimensional cosine-shape model to estimate the wake turbulence intensity; they assumed that the wake has a similar growth rate in the spanwise and vertical directions and that the maximum added turbulence intensity is redistributed along the radial direction with a dual-cosine shape function.

$$\Delta TI(x,y,z) = \delta(z).I_{+,m}(x) \begin{cases} \cos\left(\dfrac{\pi}{2}.\dfrac{r-\frac{D}{2}}{r_w-\frac{D}{2}}\right) & \frac{D}{2} < r < r_w \\ \cos\left(\dfrac{\pi}{2}.\dfrac{r-\frac{D}{2}}{r_w}\right) & 0 < r < \frac{D}{2} \end{cases} \tag{5}$$

$$\delta(z) = \begin{cases} \sin\left(\pi \dfrac{H-z}{D}\right) & z < H \ \ \& \ \ r < r_w, \\ 0 & else, \end{cases} \tag{6}$$

where r_w and $I_{+,m}(x)$ are functions of C_T, TI_∞, and $(\frac{x}{D})$ of the form $aC_T^b TI_\infty^c (\frac{x}{D})^d$.

Wind turbine wakes have also been studied with numerical wake models. The first numerical wake model was proposed by Lissaman (1979), who pre-dated Jensen (1983) and developed a numerical program to solve the complex problem of overlapping wakes in an array of multiple wind turbines. Lissaman (1979) was the first to recognize the importance of ambient turbulence in overlapping wakes, which, he stated, may have a greater impact than that due to the momentum deficit generated

by the individual turbines. Over ten years later, Ainslie (1988) proposed a numerical solution for the wake development by simplifying the Navier-Stokes equations for the turbulent boundary layer and introduced ambient turbulence and its effect on the wake decay. More recently, Yang et al. (2015) proposed a modeling framework of ΔTKE by a wind turbine in vertical planes downwind as a function of inlet velocity at hub height and thrust coefficient, which can be used to estimate the TKE of turbine wakes in complex terrain.

Whether purely analytical or numerical, whether predicting wind speed deficit or added turbulence intensity or both, wake models are useful to understand the behaviour of a wind turbine wake, but they cannot provide any information on the effects of the wake on the surrounding environment, such as changes in vertical mixing, or surface temperature, or heat and momentum fluxes at the surface. Large-eddy simulation (LES) has been a successful numerical approach to study wind turbine wakes (Breton et al., 2017) and their effects on the surrounding environment (Wu et al., 2023) because of their high spatial and temporal resolutions (order of a few meters and tens of seconds, respectively) and the accuracy of the actuator disk (Sørensen and Myken, 1992; Madsen, 1996; Mikkelsen, 2003) and actuator line (Sorensen and Shen, 2002) models used to incorporate the effects of the rotating blades. Many LES studies have been conducted to capture wind speed and TKE properties in wind turbine wakes (Eriksson et al., 2015; Vanderwende et al., 2016; Lee and Lundquist, 2017; Deskos et al., 2019; Siedersleben et al., 2020; Feng et al., 2022). Notably, Wu et al. (2023) conducted LES that included the effect of atmospheric stability to show that the wind speed deficit behaves differently from ΔTKE (e.g., the wind speed deficit reaches the ground within 8D while added TKE remains aloft) and that the two are not co-located in the wake region (e.g., the wind speed deficit peaks at hub height while added TKE near the rotor tip). However, LES are computationally demanding and therefore are not used for medium- or long-term wind farm power predictions, but rather for temporal horizons of the order of a few hours to a day.

Numerical weather prediction (or mesoscale) models, like the Weather Research and Forecast (WRF) (Skamarock et al., 2021), are the preferred tool to predict weather over longer temporal horizons, from several days to several years. However, due to the coarser spatial resolution than that of LES, ranging between 1 to 100 km, numerical weather prediction models cannot resolve the details of the wind turbine wakes, which therefore need to be "parameterized." A parameterization is a way to include the effects of a process of interest that cannot be resolved directly by the numerical model, typically because the spatial resolution of the numerical model is not fine enough to explicitly treat that process. A parameterization is basically a model-within-a-model that uses the resolved variables at each grid cell to calculate the effects of the process of interest on the resolved variables in that cell (but not the process itself). In the WRF model, several processes are parameterized, including convection, boundary layer turbulence, radiation, to name a few. The wind farm parameterization (WFP) available by default in WRF is that by Fitch et al. (2012), which treats the wind turbines in a grid cell as sinks of momentum and sources of TKE. As shown in the literature (Pan and Archer, 2018; Archer et al., 2019, 2020; Fischereit et al., 2022), the Fitch parameterization ignores wake effects within a grid cell and treats ΔTKE in an overly simplistic way.

In summary, most studies in the literature have focused on predicting the velocity deficit caused by wind turbines; far fewer have focused on added turbulence. In the far-wake region, which is the most relevant portion of the wake for long-term impacts on the environment, TKE is formed due to the increased shear caused by the wind speed deficit in the upper part of the rotor area. If ΔTKE is not accounted for properly, inaccurate predictions of the turbulent fluxes of heat and momentum near the

surface may occur, which ultimately may cause inaccurate predictions of near-surface temperature and moisture. Here, we aim at developing an analytical formulation for ΔTKE by wind turbines that is designed to be ultimately incorporated in a future wind farm parameterization for the WRF and other numerical weather prediction models. With the understanding that any parameterization is, by definition, an approximation, our goal in this paper is to propose a reasonable analytical formulation for added TKE that avoids over-prediction. Avoiding over-prediction of added TKE is crucial for a (future) parameterization because a numerical mesoscale model, like the WRF, will add some TKE on its own due via the production term in the TKE equation, due to the weak, additional, resolved vertical shear caused by the reduced wind speed in the grid cell of the turbines. If the parameterization over-estimates TKE in addition to the TKE added from the resolved shear, then an excess of TKE will occur. This issue of potential "double counting" of TKE was first addressed by Ma et al. (2022b, a). Our formulation for ΔTKE is inspired by that proposed by Ishihara and Qian (2018), as their analytical formula for added turbulence intensity by a wind turbine depends on atmospheric stability (via ambient turbulent intensity) and turbine technical specifications (via the thrust coefficient).

2 Methods

TKE is the kinetic energy per unit mass associated with eddies in a turbulent flow, defined as half of the sum of the variances (squares of standard deviations) of the three velocity components u, v, and w (along x, y, and z, respectively) as follows:

$$TKE = \frac{1}{2}\left(\sigma_u^2 + \sigma_v^2 + \sigma_w^2\right) = \frac{1}{2}\left(\overline{u'^2} + \overline{v'^2} + \overline{w'^2}\right), \tag{7}$$

where a bar $\overline{(\cdot)}$ indicates a mean and a prime $(\cdot)'$ refers to a fluctuating component, i.e., the difference between the instantaneous and the mean wind component, e.g., $u' = u - \bar{u}$.

Turbulence intensities are defined along each direction as follows (Arya, 2001; Burton et al., 2011):

$$TI_x = \frac{\sigma_u}{\overline{U}} = \frac{\sqrt{\overline{u'^2}}}{\overline{U}}, \quad TI_y = \frac{\sigma_v}{\overline{U}} = \frac{\sqrt{\overline{v'^2}}}{\overline{U}}, \quad TI_z = \frac{\sigma_w}{\overline{U}} = \frac{\sqrt{\overline{w'^2}}}{\overline{U}}, \tag{8}$$

where $\overline{U}$ is the mean wind speed, generally taken at hub height and often only horizontal. If turbulence was truly isotropic, then the three standard deviations should be approximately equal to one another. In the real atmosphere, however, where the x, y, and z axes are aligned with the west-east, south-north, and bottom-up directions, respectively, this is not true. Typically the largest one is σ_u, followed by σ_v (approximately 0.64–0.75σ_u in neutral conditions) and then by σ_w (approximately 0.50–0.52σ_u in neutral conditions) (Arya, 1988; Stull, 2017).

In the wind energy community, since wind turbines are generally yawed to face the mean wind, the x direction is set to coincide with the longitudinal (or streamwise) direction (which is not necessarily aligned west-east), and the y and z directions are denoted as lateral and upward. The International Electrotechnical Commission (IEC) standard for wind turbines (International Electrotechnical Commission, 2019) defines turbulence intensity as "the ratio of the wind speed standard deviation to the mean wind speed," but it effectively considers only σ_u (referred to as σ_1 or "turbulence standard deviation", where 1 is the index for the x-axis) in its definition of TI. However, the IEC standard recognizes that the three standard deviations in Eq. 8 should

be different from one another and recommends that any wind velocity field for turbulence models used for standard turbine classes satisfy the following conditions: $\sigma_v \geq 0.7\sigma_u$ and $\sigma_w \geq 0.5\sigma_u$.

There is not a straightforward relationship between σ_U and the standard deviations of the individual wind components σ_u, σ_v, and σ_w because of the non-linear relationship $U = \sqrt{u^2 + v^2 + w^2}$. It can be shown that, to a first approximation, the standard deviation of the wind speed σ_U is close to that of the streamwise component σ_u (Larsén, 2022), which supports the convention used by the IEC. In light of these considerations, here we define TI as the ratio of the wind speed standard deviation over the mean wind speed at hub height, but use the following approximations:

$$TI = \frac{\sigma_U}{\overline{U}} \approx \frac{\sigma_u}{\overline{U}} \approx \frac{\sqrt{\frac{2}{3}TKE}}{\overline{U}} \tag{9}$$

Traditionally, only the horizontal wind speed is used for U and $\overline{U}$, possibly because only the horizontal components of wind velocity contribute to the rotation of the wind turbine blades. The approximate relationship between TI and TKE in Eq. 9 (Wilcox, 2006), which is based on the assumption of isotropic turbulence and is therefore likely to overestimate TI, is used to convert between TI and TKE when needed (e.g., in the Validation Section 3.2). In particular, the relationship used in this study between added TI (ΔTI) and added TKE (ΔTKE) is:

$$\Delta TI = \sqrt{\frac{2}{3}}\,\frac{\Delta TKE}{\overline{U}} = \sqrt{\frac{2}{3}}\,\frac{TKE - TKE_\infty}{\overline{U}}, \tag{10}$$

where TKE_∞ is, broadly speaking, the free-stream turbulent kinetic energy. The exact definition of TKE_∞ depends on the type and distribution of the available data. If three-dimensional simulation data are available from a run without turbines (i.e., a precursor run) and a run with turbines, then the point-by-point difference of the time-averaged TKE of the two runs is used to calculate ΔTKE, e.g., for the validation LES datasets described in Section 2.2. If only a simulation with turbines is available, as is the case for the validation LES datasets described in Section 3.2, then the vertical profile of TKE at an upstream distance of $x = x_0 - 2D$ is obtained by calculating at each level the average of TKE over $-3D \leq y - y_0 \leq +3D$, where x_0, y_0 are the coordinates of the turbine. The value of TKE_∞ to use at each point downstream is, then, the value of TKE in the upstream vertical profile at the same vertical level.

A notable difference between Eqs. 7 and 9 is that TKE includes the vertical fluctuations of the wind field, which makes TKE more suitable than TI for applications where vertical mixing is important, like wind turbine wake effects. In addition, in mesoscale models like the WRF, TKE is often a prognostic variable that is directly simulated, whereas neither TI nor the standard deviations of the wind components are (i.e., there is no equation to obtain directly the individual components of the Reynolds stress tensor). In the field, however, it has been common to compute TI from measurements because TI can be calculated from simple and relatively inexpensive two-dimensional cup anemometers (thus only the horizontal components are considered), whereas sophisticated and expensive three-dimensional sonic anemometers are necessary to measure all three components of the wind in order to derive TKE.

In the rest of this study, x is the downstream distance from the wind turbine, z is vertical distance from the ground, and y is lateral distance from the wind turbine (positive to the left of the turbine, facing the turbine).

2.1 Proposed formulation

The equation for added TI by Ishihara and Qian (2018) is the starting point of the proposed formulation because it captures well the annular distribution of turbine-induced turbulence and its evolution into a single-peak Gaussian with distance. A few features, however, are not well resolved: the peak of added turbulence at hub height occurs at about 1D from the turbine position, rather than at 4-6D where shear production is highest; the peak in the vertical at the rotor top is too strong; and a spurious peak forms below the rotor. Inspired by the formulation of Ishihara and Qian (2018), but with the intent of improving upon the issues above, here we propose that ΔTKE, normalized by the square of the upstream undisturbed hub-height wind speed U_∞, can be modeled as the product of three functions: a streamwise function $A(x)$, a radial function $G(r)$, and a vertical function $W(z)$:

$$\frac{\Delta TKE}{U_\infty^2} = \alpha \times A(x) \times G(r) \times W(z). \tag{11}$$

We note that the formulation by Ishihara and Qian (2018) was similar, except it did not include a $W(z)$ function. The scalar α is a tuning parameter that ensures that the amplitude of $\Delta TKE/U_\infty^2$ in the wake is of the right magnitude (i.e., matches the LES data, as described later).

The streamwise function $A(x)$ should not be exponentially decreasing, as often assumed for turbulence intensity (Quarton and Ainslie, 1990; Crespo and Hernández, 1996; Xie and Archer, 2015; Ishihara and Qian, 2018), because ΔTKE is well-known to peak at a distance x_{max} between 4D and 8D from the turbine's streamwise location x_0 (Xie and Archer, 2015; Wu et al., 2023), not at x_0 (Fig. 1a). Here we propose a Weibull-like distribution for $A(x)$ as follows:

$$A(x) = \left(\frac{x - x_0}{\lambda_A}\right)^{k_A - 1} exp\left[-\left(\frac{x - x_0}{\lambda_A}\right)^{k_A}\right], \tag{12}$$

where λ_A and k_A are the scale and shape parameters of the Weibull distribution. The Weibull function is chosen because it is non-symmetric and because it is one-tailed, as is the observed distribution of added TKE along x. The Weibull distribution was also recently proposed for the x-dependency of added TI by Delvaux et al. (2024, their Eq. 3). We set $k_A = 2$ to reduce the overall number of parameters to fit and to obtain a function with the desired properties, i.e., equal to zero at x_0 (thus $k_A > 1$) and rapidly increasing past x_0, but not too rapidly (which would be the case for $k_A < 2$). An example of the evolution of $A(x)$ is shown in Fig. 1a in blue.

The radial function $G(r)$ is assumed to be a Gaussian that peaks at the tip annulus of the rotor, inspired by the $\phi(r)$ function of Ishihara and Qian (2018), as follows:

$$G(r) = \exp\left[-\frac{(r - D/2)^2}{2\sigma_r^2}\right], \tag{13}$$

where r is:

$$r = \sqrt{(y - y_0)^2 + (z - H)^2}, \tag{14}$$

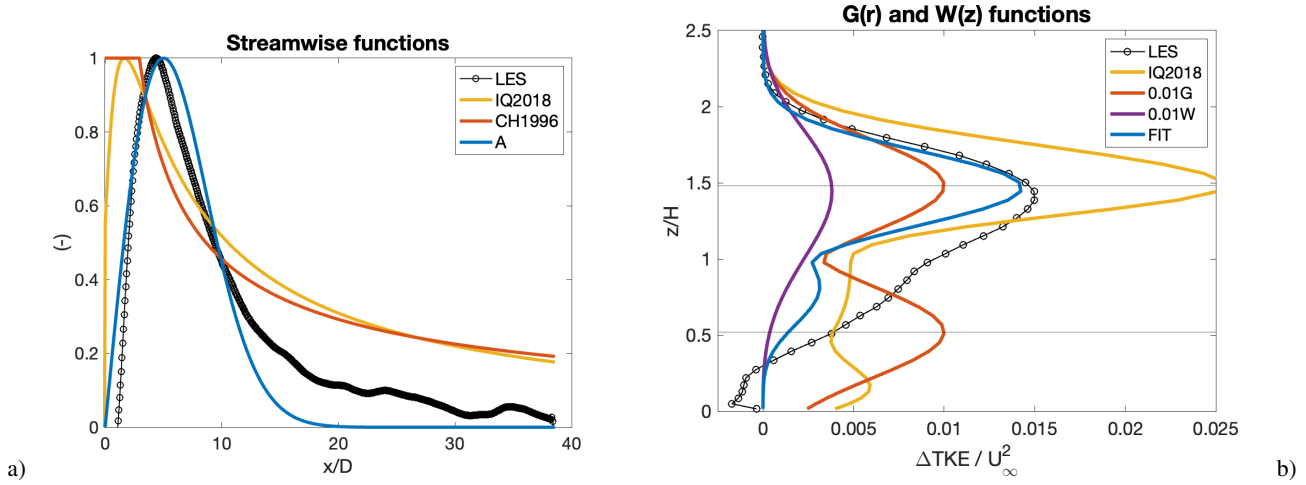

Figure 1. Comparison of the proposed fitting functions against the WRFLES-N results by Wu et al. (2023) (labeled 'LES'): a) streamwise function $A(x)$ at $z = H$ and $y = y_0 + D/2$ versus the fit by Ishihara and Qian (2018) ('IQ2018') and by Crespo and Hernández (1996) ('CH1996'), and b) radial and vertical functions $G(r)$ and $W(z)$ at $x = x_0 + 5D$ and $y = y_0$. Note that $G(r)$ and $W(z)$ are re-scaled for displaying purposes. The grey thin lines in b) indicate the rotor top and bottom.

y_0 is the spanwise location of the turbine, and σ_r is a linear function of x:

$$\sigma_r(x) = k_r\,(x - x_0) + \varepsilon_r D, \tag{15}$$

where k_r is the radial expansion rate (i.e., $\frac{\partial \sigma_r}{\partial x}$) and ε_r is a multiplying factor to the rotor diameter that sets the initial width of the Gaussian distribution of the added TKE along the annulus of the rotor disk.

Lastly, the vertical function $W(z)$ is also assumed to be Weibull-like:

$$W(z) = \left(\frac{z}{\lambda_W}\right)^{k_W - 1} exp\left[-\left(\frac{z}{\lambda_W}\right)^{k_W}\right], \tag{16}$$

where the shape parameter k_W is set equal to 4 after a trial-and-error process to ensure a steeper decrease in ΔTKE above the top tip than below it, as shown in the LES results. Examples of vertical profiles of the functions G and W are shown in Fig. 1b with yellow and orange lines.

Due to the properties of the Weibull distribution, there is an analytical relationship between the point at which the function reaches the maximum, which by definition is the mode (x_m), and the value of λ:

$$\lambda = \frac{x_m}{\left(\frac{k-1}{k}\right)^{\frac{1}{k}}}. \tag{17}$$

Thus, the values of λ_A and λ_W are directly related to the position of the maximum ΔTKE along x and z, respectively. As such, it is reasonable to expect that λ_A and λ_W depend on D and H.

In summary, the equation for $\Delta TKE/U_\infty^2$ (Eq. 11) contains five unknown parameters: $\alpha, \lambda_A, \lambda_W, k_r$, and ε_r. Before we explain how we obtain their values (by fitting) and why we refer to them hereafter as the five "direct-fit" parameters (in Section 2.3), we need to describe the datasets that we used for the fitting (in the next Section 2.2).

2.2 LES datasets

We use two independent LES datasets to calibrate the fitting parameters of our analytical model (Eqs. 11-16): the published results of Wu et al. (2023) and Vahidi and Porté-Agel (2025), described next.

The modeling system used by Wu et al. (2023) included both an LES model (WRF-LES) (Moeng et al., 2007) and a generalized actuator disk parameterization (WRF-LES-GAD) (Mirocha et al., 2014). A single and a row of wind turbines were simulated under neutral, stable, and unstable conditions with different undisturbed hub-height wind speed, turbulence intensity, and thrust coefficient (Table 1). The outer domain with horizontal grid spacing of 15 m was one-way nested with an inner domain with finer horizontal grid spacing of 5 m (see their Figure 1). The vertical resolution started at 2.5 m near the ground and was then stretched by 10% per level until 35 m, kept constant at 5 m from 35 m to 200 m, and finally stretched by 5% until the model top. The lateral boundary conditions were periodic for the outer domain and time-varying for the inner domain. The time step was 1/7 s in the outer domain and 1/21 s in the inner domain. The wind turbine was the PSU 1.5-MW turbine with H = 80 m and D = 77 m, placed in the domain at 8.2D from the inlet of the inner domain and centered laterally. The temperature profile was uniform at 297.3 K up to the initial boundary layer height (at 200 m, 500 m, and 800 m for stable, neutral, and unstable conditions, respectively), with an inversion of 0.01 K m^{-1}. The desired atmospheric stability was imposed by assigning a surface heat flux of -0.07, 0, and +0.07 K m s^{-1} for stable, neutral, and unstable conditions, respectively, with a surface roughness length z_0 = 0.01 m for all simulations.

The LES results of Vahidi and Porté-Agel (2025) were obtained with the WiRE-LES solver (Abkar and Porté-Agel, 2015), with a standard actuator disk model (Meyers and Meneveau, 2010) for the axial force induced by the wind turbine. The computational domain was 3840 m $\times$ 1920 m $\times$ 640 m with 256 $\times$ 256 $\times$ 128 grid points in the x, y, and z directions, respectively, with z_0 = 0.001 m and no Coriolis force. The wind turbine, with $D = H$ = 80 m, was located at a distance of 15D from the inlet and centered laterally. The boundary conditions in the horizontal direction were periodic for the precursor (i.e., with no wind turbine) runs. When the turbine was inserted in the domain, an inflow boundary condition was applied to override the imposed periodic boundary condition in the streamwise direction using the prior periodic results. To smoothly adjust the flow to an undisturbed inflow condition, a buffer zone was introduced upstream of the inflow section. A constant streamwise pressure gradient was used to maintain a velocity of around 8 m s^{-1} at the center of the actuator disk.

Further details about the LES suites that will be used for calibration can be found in the original studies (Wu et al., 2023; Vahidi and Porté-Agel, 2025) and in Table 1.

2.3 Least-square error fitting procedures

We use the Python least-square error non-linear fitting function in two steps. First, we run the fitting separately for each of the 15 LES cases over the wake region of the various computational domains using Eqs. 11–16, to obtain 15 sets of the five

Table 1. Simulation details and values of the five direct-fit parameters for the 17 LES cases used for the analytical model calibration. The label "WRFLES" refers to the WRF-LES dataset by Wu et al. (2023), where "S", "N", and "U" refer to stable, neutral, and unstable conditions; "VPA-TI064" and "VPA-TI107" refer to the neutral-stability simulations by Vahidi and Porté-Agel (2025), with TI set to 0.064 and 0.107.

Calibration case	D (m)	H (m)	U_{hub} (m s^{-1})	C_T (-)	TI_∞ (-)	α ($\times 10^{-2}$)	λ_A (m)	λ_W (m)	k_r ($\times 10^{-2}$)	ε_r ($\times 10^{-1}$)
WRFLES-S	77	80	8.96	0.70	0.065	8.88	830	126	3.06	1.09
WRFLES-N	77	80	9.16	0.68	0.080	8.78	661	124	3.35	1.453
WRFLES-U	77	80	10.31	0.58	0.093	7.84	605	120	4.34	1.99
VPA-TI064	80	80	8.27	0.4	0.064	2.38	1022	116	1.69	0.98
	80	80	8.27	0.5	0.064	3.80	976	111	1.87	1.09
	80	80	8.27	0.6	0.064	5.62	909	106	2.05	1.2
	80	80	8.27	0.7	0.064	8.01	843	103	2.14	1.37
	80	80	8.27	0.8	0.064	11.18	765	101	2.26	1.55
	80	80	8.27	0.9	0.064	16.0	676	98	2.36	1.79
VPA-TI108	80	80	8.49	0.4	0.107	2.78	904	126	4.57	0.94
	80	80	8.49	0.5	0.107	4.25	862	124	4.23	1.16
	80	80	8.49	0.6	0.107	5.96	820	121	3.94	1.39
	80	80	8.49	0.7	0.107	8.13	762	118	3.84	1.57
	80	80	8.49	0.8	0.107	11.3	677	116	3.73	1.76
	80	80	8.49	0.9	0.107	16	572	111	3.58	1.94

direct-fit parameters $\alpha, \lambda_A, \lambda_W, k_r$, and ε_r (Table 1). We refer to them as "direct-fit" parameters to distinguish them from those obtained in the next step. We attempted to find fitted values also for k_A and k_W, but with 7 parameters we could never reach convergence of the least-square error fitting procedure. Then, we run the Python fitting again using simple functions of C_T and TI_∞ with three fitting coefficients each, described below, to obtain five functional relationships between the five direct-fit parameters and the two independent variables C_T and TI_∞.

Because it is unpractical to use a different set of fitting parameters for each case and because we want a smooth (i.e., not step-wise) transition between different values of C_T and TI_∞, we want to identify "functional relationships" of the five direct-fit parameters on a few relevant variables that are turbine- and stability-dependent. There are a few empirical formulations that have been proposed in the literature for ΔTI and that may be applicable for our purposes. These empirical formulations depend on both C_T and TI_∞ with the following general form (Quarton and Ainslie, 1990; Crespo and Hernández, 1996; Ishihara and Qian, 2018):

$$\Delta TI \propto a\, C_T^b\, TI_\infty^c. \tag{18}$$

Inspired by these well-established empirical formulations, here we propose that, of the five fitting parameters in Eqs. 12–16 ($\alpha, \lambda_A, \lambda_W, k_r$, and ε_r), three have the form shown in Eq. 18, namely α, k_r, and ε_r, while λ_A and λ_W include an additional

dependency on the relevant lengths D and H as follows:

$$\lambda_A = a\ D\ C_T^b\ TI_\infty^c, \tag{19}$$

$$\lambda_W = H + a\ D\ C_T^b\ TI_\infty^c. \tag{20}$$

Intuitively, for a wind turbine with a small diameter, the peak of added TKE occurs at a downstream distance from the tower that is shorter than that for a wind turbine with a large diameter, thus λ_A should depend on D, as in Eq. 19. Similarly, the TKE peak in the vertical occurs near the rotor top, thus at higher elevations for taller turbines than for shorter ones, which suggests a dependency of λ_W on H and D, as in Eq. 20.

In summary, the five functional relationships for the five direct-fit parameters are shown in the first row of Table 2. We note that there are now 3×5 = 15 functional coefficients a_i, b_i, and c_i, the values of which we obtain via another least-square error fitting. The results are shown in Fig. 2 and Table 2. Although the functional coefficients are empirical in nature, their values provide useful physical hints on the properties of added TKE, as discussed next.

Table 2. Functional relationships for the five direct-fit parameters. The values in parentheses are the original coefficients before manual overwriting to zero.

	α (-)	λ_A (m)	λ_W (m)	k_r (-)	ε_r (-)
Equation	$a\ C_T^b\ TI_\infty^c$	$a\ D\ C_T^b\ TI_\infty^c$	$H + a\ D\ C_T^b\ TI_\infty^c$	$a\ C_T^b\ TI_\infty^c$	$a\ C_T^b\ TI_\infty^c$
a	0.217	3.938	1.384	0.480	0.411
b	2.269	-0.472	-0.429	0 (-0.061)	0.728
c	0 (0.037)	-0.281	0.541	1.105	0.298

Starting with α (Fig. 2a), its functional relationship is extremely consistent among all the runs and independent of TI_∞, thus the value of c, originally equal to 0.037, is set to zero in Table 2 to simplify the functional relationship and reduce the number of coefficients required overall. The implication is that the magnitude of added TKE in the wake of a wind turbine is essentially independent of atmospheric properties (such as turbulence intensity or stability), but depends only on the turbine operation through its thrust coefficient.

By contrast, the fit for k_r (Fig. 2b) is basically independent of C_T, despite a weak and conflicting dependency in the direct-fitting values, thus b is overwritten as zero from the original value of -0.061 in Table 2. This indicates an interesting finding: that the radial expansion rate of the wake TKE is independent on the turbine operation but is only a function of the amount of background turbulence. This finding is consistent with the literature, as k_r has a similar meaning as the well-known expansion rate k_w (also known as just k) in the Jensen model (Jensen, 1983), which is typically set to 0.075 onshore, where background

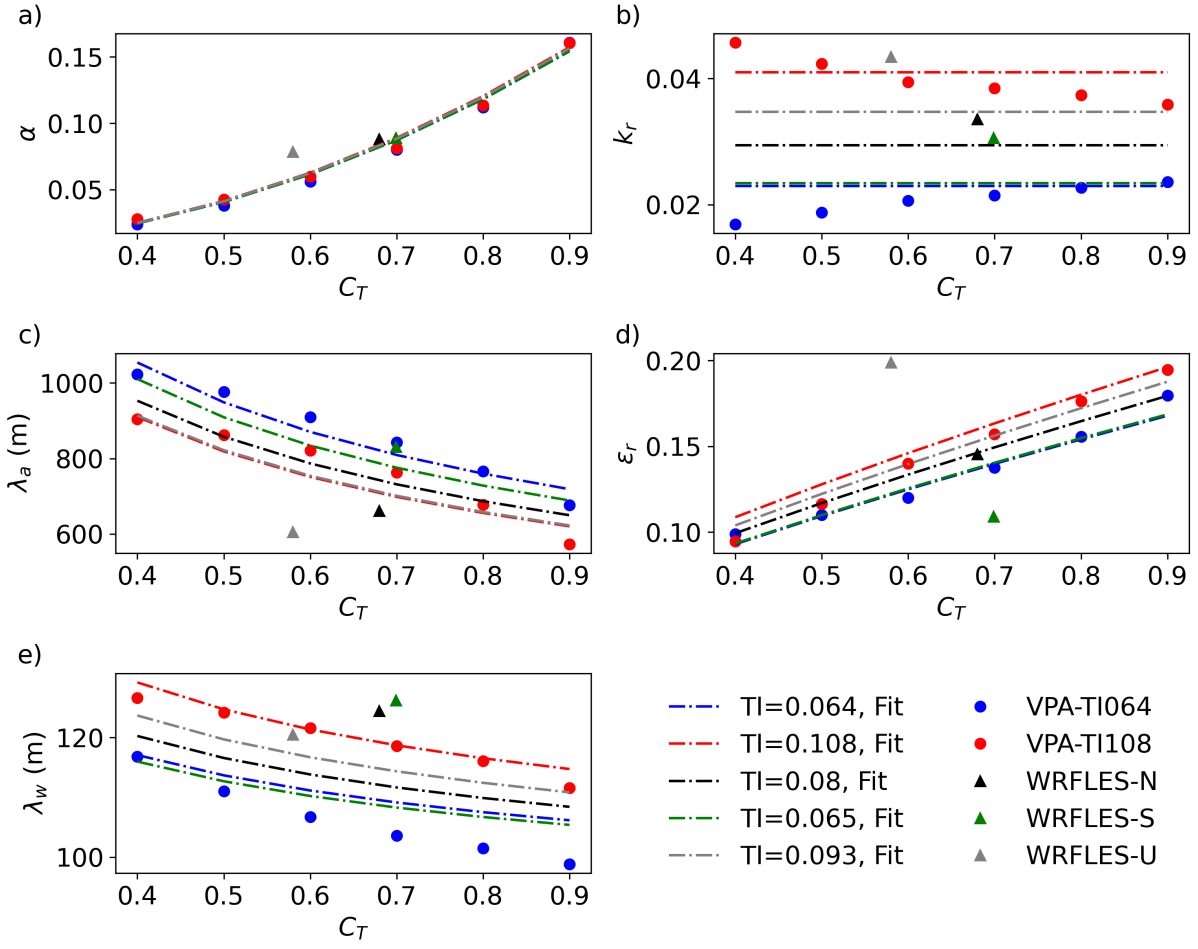

Figure 2. Performance of the functional relationships at predicting the five direct-fit parameters: a) α, b) k_r, c) λ_A, d) ε_r, and e) λ_W.

turbulence is generally high, and 0.04 offshore, where turbulence is low (Archer et al., 2018). We note that k_r is the expansion of the wake TKE, while k_w is the expansion of the wake wind speed deficit. As a result of the analysis of the functional relationships for α and k_r, the number of fitting coefficients is reduced from 15 to 13.

Next, ε_r is proportional to both C_T and TI_∞, but the dependency on C_T is stronger (b is more than twice as large as c, Table 2). Since ε_r controls the spread of the added TKE distribution along the annulus of the rotor disk, it is not surprising that its value for the unstable case (WRFLES-U) is under-predicted, while for the stable case (WRFLES-S) it is over-predicted in Fig. 2d.

Focusing on λ_A next, since the values of both b and c are negative (Table 2), λ_A is inversely proportional to both C_T and TI_∞. However, since both C_T and TI_∞ are always lower than 1 and b and c are both negative and lower than 1, but c is larger in magnitude, the dependency on TI_∞ ends up being dominant. This finding too is physically sound: everything else being

the same, the downstream peak of added TKE is expected to be closer to the wind turbine when the background turbulence is high and further downstream when the background turbulence is low, because high turbulence causes a shorter wake than low turbulence, increases mixing, and smooths down the peak.

By contrast, λ_W is inversely proportional to C_T and directly proportional to TI_∞ (Fig. 2e), consistent with negative b and positive c in Table 2. However, due to the additional dependency on H and D, the comparison between the lines in Fig. 2e needs to be conducted for the same D and H, thus only among lines of the same LES group. For example, looking at the VPA runs only, a nearly doubling of TI_∞ going from VPA-TI064 to VPA-TI108 causes an about 10-m rise in the vertical placement of the TKE peak, while a nearly doubling of C_T from 0.4 to 0.7 causes less than 5 m of drop in the peak position.

The two-step approach described so far may appear cumbersome, with an initial least-square error fit to the LES data for the five direct-fit parameters and then a second least-square error fit with the functional relationships to finally obtain the values of the 15 desired functional coefficients. A more straightforward approach would have been to put the functional relationships shown in Table 2 directly into Eqns. 12–16 and then to perform the least-square error fitting to the LES data for the 15 unknown functional coefficients. However, when we tried it, we were unable to reach convergence, possibly because the number of fitting parameters was too high (15 versus 5). We note that Ishihara and Qian (2018) used a total of 9 fitting parameters.

To assess the performance of the two-step approach, we calculate the root mean square errors (RMSE) over the entire wake regions of all calibration cases (Table 3, calibration cases only). The entire wake region covers an area with y from -1D to +1D and z from 0-2H. Please note that we have different values along the x direction as some LES cases and the experimental test only cover a small region in downstream. The proposed analytical formulation outperforms that by Ishihara and Qian (2018) in all cases, as the RMSE of both the direct and the final fit are half as large or lower as theirs on average, and up to 6 times smaller. A general trend that emerges is that the RMSE increases as both C_T and TI_∞ increase. For example, the RMSE of the VPA runs approximately doubles when TI_∞ increases from 0.064 to 0.108 and triples when C_T varies from 0.4 to 0.9. Not surprisingly, the RMSE of the final fit is always higher than that of the direct fit, as, by definition, the direct-fit parameters are those that minimize the error. We note that the RMSEs are relatively large, close to or slightly higher than the mean value of $\Delta TKE/U_\infty^2$. For example, the RMSE of the final fit for the WRFLES runs is about 1.4×10^{-3} and the mean value of $\Delta TKE/U_\infty^2$ for the same runs is about 1.3×10^{-3}.

3 Results

3.1 Comparison with LES data

First, we look at the individual functions A, G, and W along one relevant dimension for the calibration case WRFLES-N. For A, the relevant dimension is x and the proposed formulation exhibits the correct features (Fig. 1a): the function is zero at x_0, it rapidly increases and then peaks at about 6D, slightly further downstream than indicated by the LES profile, which peaks at about 5D, and then it slowly decreases to nearly zero at 20D. Both the IQ2018 and the CH1996 curves peak near or at the rotor (at $0D$) and retain too much TKE in the far wake after 10D.

Table 3. RMSE values of the 15 LES calibration cases and the four validation cases against the benchmark model proposed by Ishihara and Qian (2018), labeled as "IQ2018", the direct fit (with direct-fit parameters from Table 1) and the final fit (with the functional relationships from Table 2). The RMSEs are calculated over a longer domain for the validation cases (0D–20D) than the calibrations cases (up to 10D, see text for details).

Calibration case		IQ2018 ($\times 10^{-3}$)	TIAN2022 ($\times 10^{-3}$)	Direct fit ($\times 10^{-3}$)	Fit ($\times 10^{-3}$)	$\overline{\Delta TKE/U_\infty^2}$
WRFLES-S		3.77	9.32	1.19	1.37	1.22
WRFLES-N		3.66	8.67	1.15	1.27	1.23
WRFLES-U		3.11	8.68	1.33	1.54	1.50
VPA-TI064	C_T=0.4	1.84	0.29	0.29	0.31	
	C_T=0.5	1.89	4.71	0.37	0.40	0.21
	C_T=0.6	2.29	4.84	0.55	0.59	0.43
	C_T=0.7	3.06	4.9	0.88	0.92	0.72
	C_T=0.8	4.12	5.11	1.34	1.37	1.09
	C_T=0.9	5.4	5.22	1.98	2.02	1.61
VPA-TI108	C_T=0.4	3.38	4.34	0.70	0.71	0.13
	C_T=0.5	3.16	4.5	0.78	0.79	0.33
	C_T=0.6	3.16	4.69	0.92	0.93	0.56
	C_T=0.7	3.5	4.96	1.17	1.19	0.86
	C_T=0.8	4.22	5.2	1.54	1.56	1.24
	C_T=0.9	5.27	5.54	2.14	2.17	1.171
Validation case		IQ2018 ($\times 10^{-3}$)	TIAN2022 ($\times 10^{-3}$)	Direct fit ($\times 10^{-3}$)	Fit ($\times 10^{-3}$)	$\overline{\Delta TKE/U_\infty^2}$
XA2017		12.36	15.09	n/a	3.77	2.84
ARC2020		9.54	8.22	n/a	3.63	6.46
SOWFA		10.5	9	n/a	2.86	4.41
AJU2020		6.67	12.8	n/a	6.23	5.87

The vertical profiles of the two functions G and W (Fig. 1b) also are, for the most part, correctly reproduced by the proposed formulation, including the peak of $\Delta TKE/U_\infty^2$ near the rotor tip and the rapid decrease above it. The second peak of $\Delta TKE/U_\infty^2$ located below hub height is qualitatively reproduced but is too weak; $\Delta TKE/U_\infty^2$ below the rotor decreases without exhibiting the weak negative peak near the surface. The fit by IQ2018 greatly overestimates TKE near the rotor top (by about a factor of 2) and exhibits a spurious peak near the surface.

Next, we compare horizontal and vertical cross-sections of $\Delta TKE/U_\infty^2$ from the LES results, direct fit, and final fit for each of the three stability cases. Starting with a neutral case (VPA-TI064 with C_T=0.7) in Fig. 3, the horizontal cross sections

at hub height show that the main features and distribution of the direct and final fit for $\Delta TKE/U_\infty^2$ resemble those of the LES results, with a symmetric distribution around the wake axis and two maxima near 6D (slightly further downstream than the LES maxima at $\simeq$ 5D, as mentioned earlier for Fig. 1a). The two maxima collapse into one in the upper part of the rotor (Fig. 3, middle).

In the $x-z$ plane, the $\Delta TKE/U_\infty^2$ maximum is properly located at about 120 m above ground ($z/H \sim 1.5$); the elongated feature of higher $\Delta TKE/U_\infty^2$ extending towards the lower rotor area is more or less captured by the proposed formulation (Fig. 3, right). While the location and magnitude of the maximum, as well as the overall distribution above the rotor, are well captured by both fittings, the wake extent in the x-direction is underestimated and so is the magnitude of $\Delta TKE/U_\infty^2$ below hub height. We note that the magnitude of the maximum $\Delta TKE/U_\infty^2$ is better reproduced by the final fit than by the direct fit.

The comparison between $\Delta TKE/U_\infty^2$ from the LES and the direct and final fits under unstable conditions is also encouraging (Fig. A1 for WRFLES-U). While the direct fit closely mimics the maximum value of $\Delta TKE/U_\infty^2$ under unstable conditions across all three cross sections, the final fit underestimates this term (Fig. A1); the opposite occurred under neutral conditions in Fig. 3. However, the final fit reproduces the $\Delta TKE/U_\infty^2$ propagation along x better than the direct fit.

For stable conditions (Fig. A2), the performance of the proposed fits is more complicated. At hub height, the direct fit underestimates the magnitude of the maximum $\Delta TKE/U_\infty^2$ and the final fit improves it (Fig. A2, left). At the rotor top and in the $z-x$ plane (Fig. A2, middle and right), the opposite happens: the direct fit matches the maximum well, while the final fit underestimates it. It appears that the final fit shifts the maximum of $\Delta TKE/U_\infty^2$ further down in elevation, which causes an increase of TKE around hub height and a reduction near the rotor top.

It is important to note that we did not yet include a treatment of the hub, which causes high ΔTKE between 1D and 2D in the LES results. The well-known feature that $\Delta TKE/U_\infty^2$ extends further downstream under stable than unstable conditions is correctly captured by our proposed formulation, although the magnitude of the peak is underestimated by the fits in both cases.

Lastly, we compare the vertical and horizontal profiles of $\Delta TKE/U_\infty^2$ from the proposed final fit against the formulation of Ishihara and Qian (2018) (IQ2018) and the LES results of Wu et al. (2023) under neutral, stable, and unstable conditions at different downstream distances (Fig.4).

In general, IQ2018 overestimates the LES results, especially the magnitude of the $\Delta TKE/U_\infty^2$ peak in the near wake in the vertical (by a factor of 2, Fig.4a) and in the horizontal (by a factor of 3, Fig.4b). Large overestimates by the IQ2018 model have also been reported recently by Bastankhah et al. (2024) in the near- and far-wake regions. By contrast, the proposed fit tends to underestimate the maxima in the near wake by up to 30%. In the far wake, the proposed formulation predictions are closely aligned with the LES results; the overestimation by IQ2018 is reduced, but a secondary spurious maximum appears near the surface. Since the LES results include the effect of the hub, while both the final fit and the IQ2018 formulation do not, they both miss the peak in $\Delta TKE/U_\infty^2$ at $x = 2D$ caused by hub (Fig. 3–A1, left and right sub-figures).

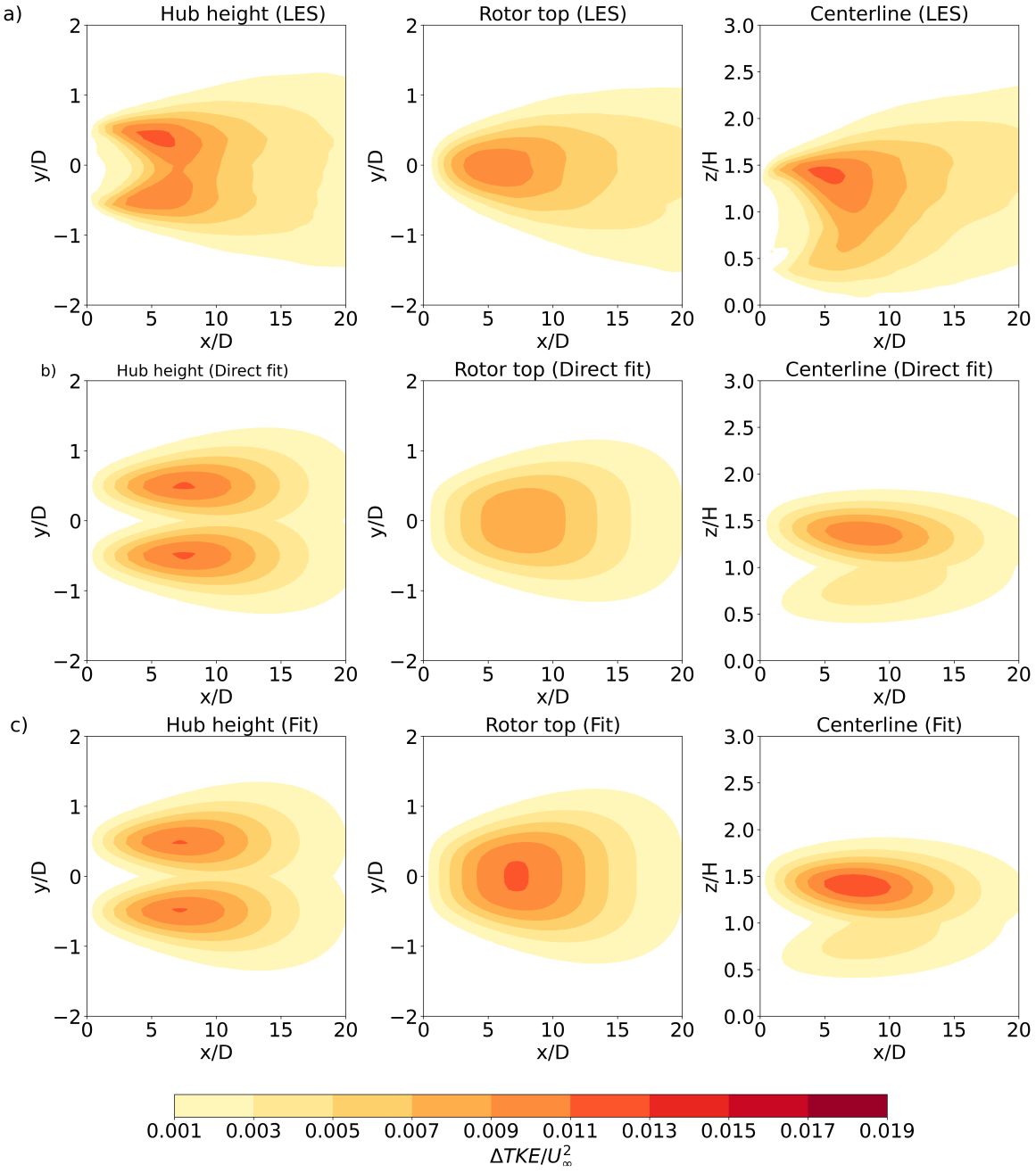

Figure 3. Cross-sections of $\Delta TKE/U_\infty^2$ under neutral conditions: a) LES (VPA-TI064 with CT=0.7), b) direct fit, and c) final fit in the $x-y$ plane at hub height (left), $x-y$ plane at the rotor top (middle) and in the $x-z$ plane at $y=y_0$ (right).

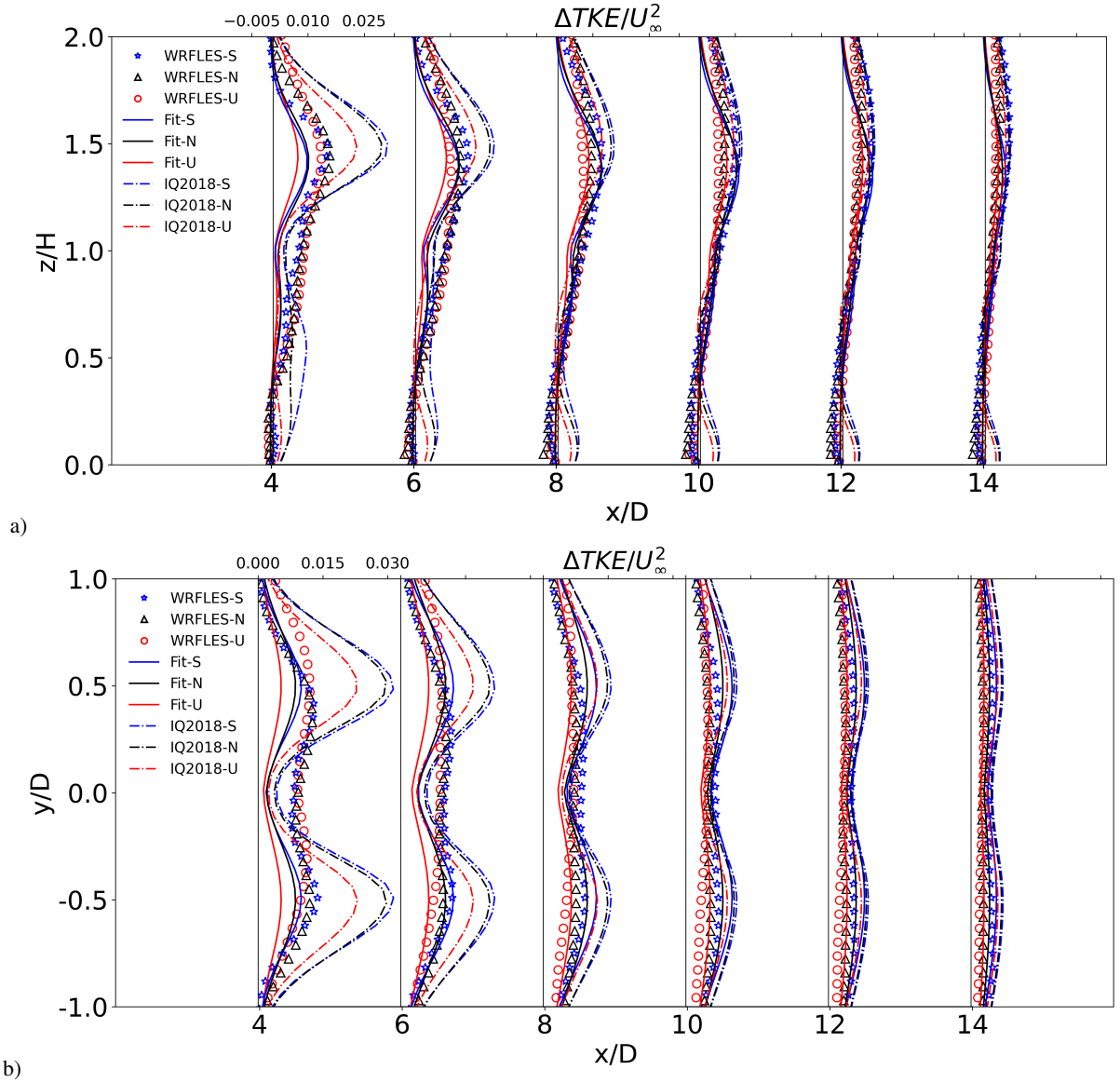

Figure 4. Profiles of $\Delta TKE/U_\infty^2$ from the proposed formulation ("Fit") and from the WRFLES runs (Table 1) along: a) z and b) y at different downstream distances.

3.2 Validation

In this section, we compare the performance of the proposed formulation for $\Delta TKE/U_\infty^2$ (i.e., with the final fitting coefficients from Table 2) with data from four other independent studies: the LES studies by Xie and Archer (2017) and by Archer et al. (2020), referred to hereafter as "XA2017" and "ARC2020," respectively; a modified version of the LES by Archer et al. (2013) and Ghaisas et al. (2017), referred to hereafter as "SOWFA;" and the wind tunnel measurements by Aju et al. (2020), referred

to as "AJU2020." The four studies are introduced and discussed below and their relevant parameters are listed in Table 4. The RMSEs for the validation cases are calculated over their respective entire domains starting at 0D to the last point available, which is different in each case (e.g., 10D for SOWFA but just 4D for AJU2020).

Table 4. Details of the datasets used for the analytical model validation. The label "XA2017" refers to the unstable LES results by Xie and Archer (2017), "ARC2020" to the neutral LES results of Archer et al. (2020), "SOWFA" to a modified version of the LES results by Archer et al. (2013) and by Ghaisas et al. (2017), and "AJU2020" to the neutral wind tunnel experiments of Aju et al. (2020).

Case	Type	Stability	D (m)	H (m)	U_{hub} (m s^{-1})	C_T (-)	TI_∞ (-)
XA2017	LES	Unstable	126	87.6	8.35	0.8	0.082
ARC2020	LES	Neutral	126	90	9	0.83	0.102
SOWFA	LES	Stable	93	80	8.3	0.8	0.074
AJU2020	Wind tunnel	Neutral	0.2	0.2	6.43	0.585	0.120

XA2017 used the Wind Turbine and Turbulence Simulator (WiTTS) (Xie and Archer, 2015), an in-house flow solver developed at the University of Delaware, for the flow simulation. WiTTS solves the unsteady, filtered three-dimensional Navier-Stokes equations in the incompressible form using the fractional method (Kim and Moin, 1985) and can handle non-neutral stabilities (Xie and Archer, 2017). The wind turbine, modeled as an actuator line (plus the nacelle), was the REpower 5-MW, with a hub height of 87.6 m and a rotor diameter of 126 m. The simulation was divided into two stages: a precursor stage (without turbines) and a formal stage (with the inclusion of five wind turbines). The five turbines were arranged in a staggered layout with along-wind spacing of approximately 1000 m (which is roughly 8D) and across-wind spacing of roughly 4D. The resolution was 6.25 m in all directions and the surface roughness length was 0.016 m. Only the wake field of the front-row turbine (labeled "WT1" in their Figure 7) from 2D to 8D is used here, to avoid contamination from the wakes of nearby turbines.

Looking at the results from the unstable run of XA2017, $\Delta TKE/U_\infty^2$ from the proposed fit matches the LES satisfactorily in the vertical and in the horizontal (Figure 5a and b), with the maximum $\Delta TKE/U_\infty^2$ of the right magnitude and correctly located at the upper part of the rotor tip at 4D and 6D. However, at 8D, the profile along the z direction shows an overestimation in predicting the maxima near the rotor tip, while correcting reproducing the profile below hub height. The RMSE is larger than that of any of the studies used for calibration, 3.77×10^{-3} (Table 3), possibly because the LES included the effect of the nacelle while both analytical formulations do not. The RMSE of the proposed fit is, however, significantly lower than that of IQ2018 (12.36×10^{-3}), which overestimates added TKE at all distances, but especially in the near wake, and introduces, again, an unrealistic peak near the ground.

The second LES study used here for validation is ARC2020 (Archer et al., 2020), in which the LES flow solver Software for Wind Farm Applications (SOWFA) was used with an actuator line model for the wind turbine blades without any treatment for the hub (Churchfield et al., 2012; Archer et al., 2013). The computational domain size was 3000 m $\times$ 3000 m $\times$ 1020 m

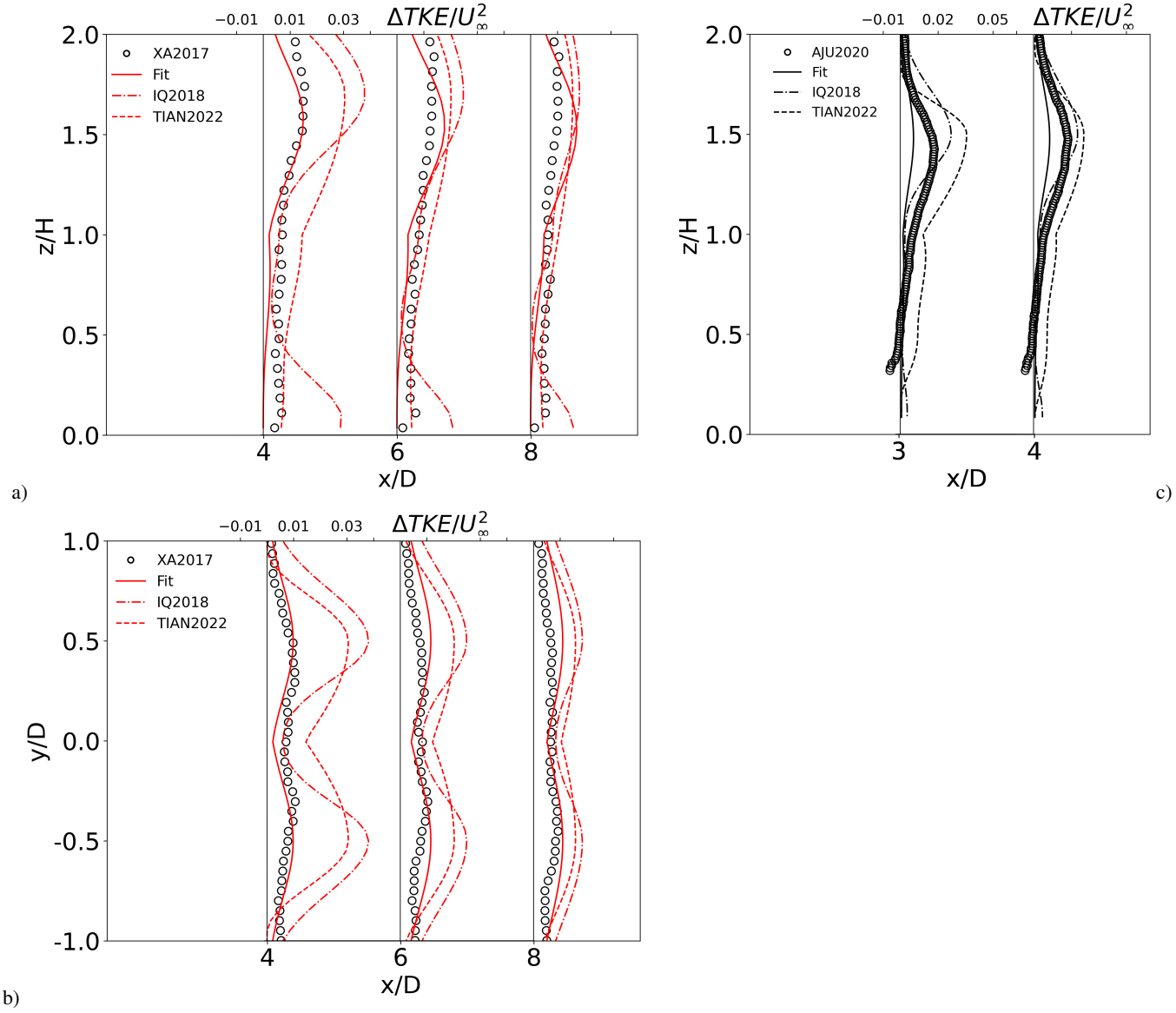

Figure 5. Profiles of $\Delta TKE/U_\infty^2$, taken at different downstream distances, from the proposed formulation, labeled as "Fit", and from: the LES dataset of XA2017 along: a) the z direction at the centerline, and b) the y direction at hub height, under unstable conditions; and c) the wind tunnel PIV measurements of AJU2020, along the z direction at the centerline, under neutral stability. The same profiles from IQ2018 and TIAN2000 are added for comparison.

with a single wind turbine in the middle and the atmospheric stability was neutral. An idealized NREL 5-MW wind turbine was used with D = 126 m and H = 90 m. The resolution was set to 200 $\times$ 200 $\times$ 68 grid points in x, y, and z, respectively, corresponding to grid cells of approximately 15 m in both horizontal dimensions.

The vertical profiles of $\Delta TKE/U_\infty^2$ from the final fitting match very well those from the LES just after $x = 2D$ (Figure 6a). We note that the slight reduction in TKE near the surface shown in the LES results, which has been observed and simulated in the literature (Archer et al., 2019; Wu and Archer, 2021), is not reproduced with the proposed fit because it is not accounted for in its equations yet. A way to account for it in the future could be via a correction similar to the δ function of IQ2018, shown here in Eq. 6. Conversely, IQ2018 shows some spurious $\Delta TKE/U_\infty^2$ below the rotor, which is not correct. The y-profiles (Figure 6b) are characterized again by a general underestimation and overestimation of the $\Delta TKE/U_\infty^2$ maxima for proposed fit and for IQ2018, respectively. The proposed fit shows a significantly improved $\Delta TKE/U_\infty^2$ profile compared to IQ2018, providing a more satisfactory prediction that closely matches the LES results starting at $x = 4D$. This validation dataset is well reproduced by the proposed formulation, with an RMSEs of 3.63×10^{-3}, about half of the average value of $\Delta TKE/U_\infty^2$ (6.46×10^{-3}, Table 3, possibly because this LES study did not include a treatment for the hub.

The third study used for validation, named SOWFA, is a modification of those by Archer et al. (2013) and by Ghaisas et al. (2017), which used the SOWFA solver over a complex mesh of 4000 m $\times$ 4000 m $\times$ 1000 m with fine refinement (about 3.5 m) in six blocks around up to 48 wind turbines (Siemens 2.3 MW with D=93 m and H=63.4 m) and coarser (7 m) in the rest of the domain. Various cases were simulated, varying the number of turbines, their layout, and the atmospheric stability. Here we use an additional stable case, with the same temperature decrease at the bottom boundary of -0.25 K h^{-1} as in Ghaisas et al. (2017), the same layout as "Stg-2SpaX" in Archer et al. (2013), but with westerly flow. To maximize the extent of the wake at fine resolution, we extracted the flow details from the wake of turbine n. 36 (see Fig. 1f in Archer et al. (2013)), approximately 10D in length.

The proposed fit provides a satisfactory match to the LES profiles, particularly in the z-profiles, in the entire domain, while a noticeable gap between the LES data and IQ2018 still exists in the near wake. We note that the stable LES results show an asymmetry in the y-profiles (Figure 7b), due to the Coriolis force and the resulting Ekman-spiral effect, which is not captured by the proposed formulation and therefore an overestimation by the final fitting can be seen in the far wake. Because this LES dataset did not simulate the effect of the hub, the RMSE was relatively low: 2.86×10^{-3}, for an average value of $\Delta TKE/U_\infty^2$ of about 4.41×10^{-3} (Table 3).

The fourth study used for validation is AJU2020 (Aju et al., 2020), which describes the Boundary Layer and Subsonic Tunnel (BLAST) experiments that were conducted at the University of Texas at Dallas. The wind tunnel is 30 m long, 2.1 m high, and 2.8 m wide, with cubic blocks of 2.5 cm of height located at 0.2 m between each other on the bottom surface of the test section to achieve a well-developed turbulent boundary layer. Horizontal axis wind turbines, with D = 200 mm and H = 200 mm, were used in the experiments, based on models from Sandia National Labs and locally manufactured at the university. A particle image velocimetry (PIV) system was used to measure the turbulence along the center axis of each turbine. The tests were conducted in neutral stability and only vertical profiles at selected downstream distances were available. Values near the surface are not reliable due to ground effects.

Comparison of the $\Delta TKE/U_\infty^2$ behind the wind turbine against the experimental data by AJU2020 under neutral conditions indicates that the proposed fit is qualitatively correct but exhibits a large underestimation of the upper rotor peak by over 100% (Figure 5c). Not surprisingly, the AJU2020 dataset is associated with the largest RMSE among the four cases used for

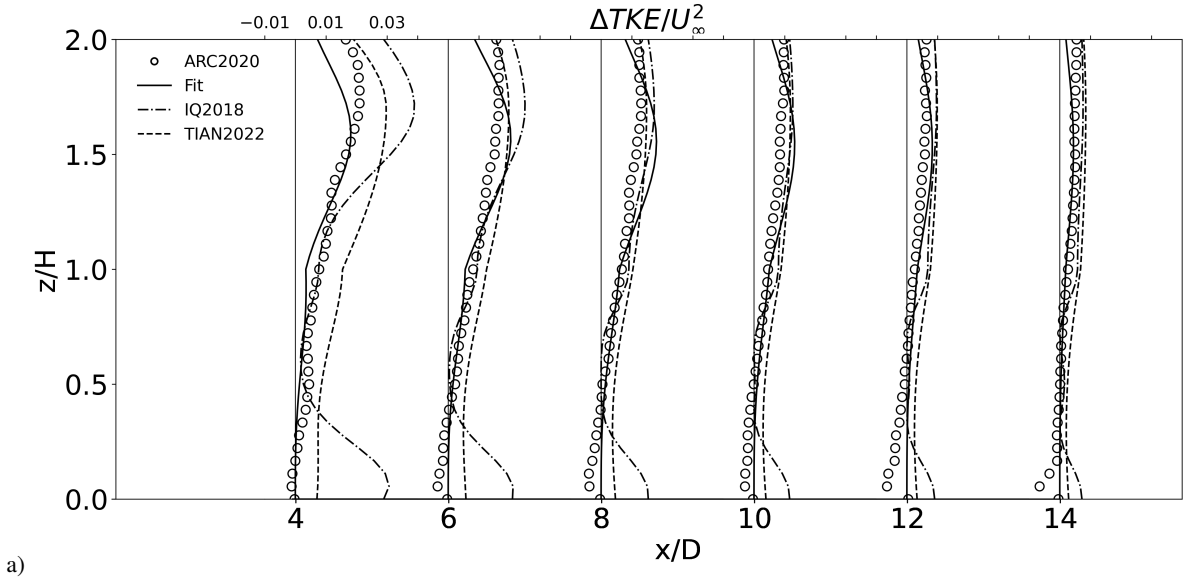

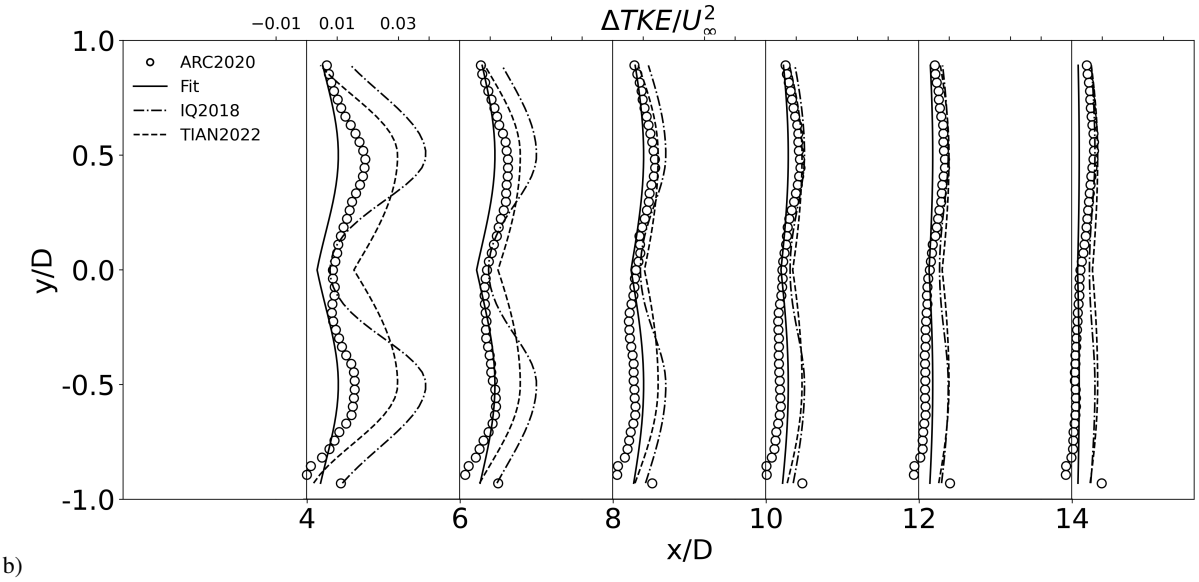

Figure 6. Profiles of $\Delta TKE/U_\infty^2$, taken at different downstream distances, from the proposed formulation, labeled as "Fit", and from the LES dataset of ARC2020 under neutral stability along: a) the z direction at the centerline, and b) the y direction at hub height. The same profiles from IQ2018 and TIAN2000 are added for comparison.

validation, exceeding 6×10^{-3} for an average value of $\Delta TKE/U_\infty^2$ of 5.87×10^{-3} (Table 3). This is possibly explained by the fact that this experimental dataset just covers a small region behind the turbine, between $x = 0 - 4D$, where the effect of the hub is more significant. By contrast, this is the only dataset that compares well against the IQ2018 predictions, despite an overestimation of the maximum at 3D and an overall RMSE still larger than that of the proposed fit (6.67×10^{-3}, Table 3).

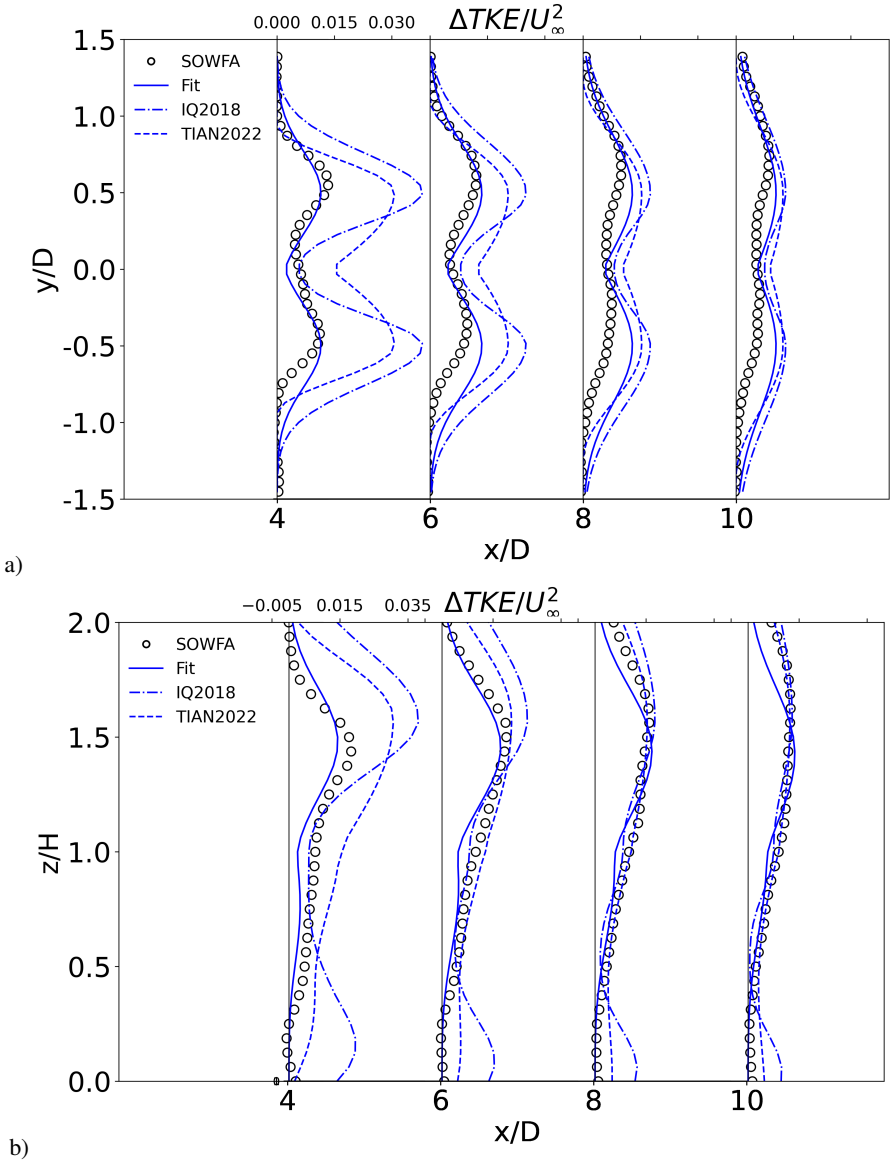

Figure 7. Same as Figure 6, but for the SOWFA LES dataset under stable conditions.

4 Conclusions and recommendations

This study is a first step in addressing the lack of a proper treatment of the turbulence added by wind turbines in current numerical weather prediction models, like the WRF model. An analytical formulation for $\Delta TKE/U_\infty^2$ is presented, comprising five fitting parameters, each with a functional relationship with the thrust coefficient of the turbine, the undisturbed upstream turbulence intensity, the diameter, and the hub height of the wind turbine. The fitting parameters are obtained after a two-step

fitting process based on the LES dataset from a previous study by Wu et al. (2023)), which used the WRF-LES code for three atmospheric stability cases (stable, neutral, and unstable), and from 15 LES cases in neutral stability with various combinations of TI_∞ and C_T by Vahidi and Porté-Agel (2025).

The proposed formulation compares well with the LES datasets that were used for the parameter calibration, which is to be expected, with RMSEs of the same order of magnitude as the mean $\Delta TKE/U_\infty^2$, but it is less accurate when compared against four additional and independent datasets used for validation: an LES study of a 5-MW wind turbine under unstable conditions using the WiTTS code (Xie and Archer, 2017), another LES study of the same 5-MW wind turbine under neutral stability using the SOWFA code Archer et al. (2020), another SOWFA run under stable conditions Archer et al. (2013); Ghaisas et al. (2017), and a wind tunnel experiment with a model wind turbine under neutral conditions Aju et al. (2020).

We conclude that the proposed formulation is promising at predicting the distribution of $\Delta TKE/U_\infty^2$ under all stabilities in the far-wake, which is the more relevant region for mesoscale studies of the impacts of wind farms on the environment. In the near-wake, the blade geometry, rotor tip, and hub effects have a dominant effect on $\Delta TKE/U_\infty^2$ and the proposed formulation performs worse there than in the far-wake. However, the proposed formulation outperforms that by Ishihara and Qian (2018) in all cases.

The ultimate goal of this research is to eventually insert the $\Delta TKE/U_\infty^2$ formulation, after further improvements to better capture the near-wake behavior, in numerical weather prediction models to better quantify the possible impacts of wind turbine wakes on the environment. However, in order for the proposed formulation to be effectively used for this purpose, the total ΔTKE in each grid cell of the mesoscale model needs to be calculated, but the volume-integral of Eq. 11 cannot be obtained analytically. As such, numerical integration is required, which may add a small computational cost to the simulation. In addition, in the presence of multiple wind turbines with multiple overlapping wakes, the issue of superposition of wake-added TKE needs to be resolved.

We note that we did not include a treatment of either the nacelle or the tower in our formulation, which, combined, were found to have an effect on the wake dynamics that was larger than previously thought, in the case of a model wind turbine in a wind tunnel (Santoni et al., 2017). Since only XA2017 included the nacelle in their simulation, while none of the validation or calibrations studies included the tower, we neglected both for now.

Another limitation of our formulation is that its calibration relies on LES results, which introduce several uncertainties, from the sub-grid turbulence closure model to the sampling method for the actuator line model (Martínez-Tossas et al., 2017). Using only real measurements would not remove all uncertainties either, as measurements have their own intrinsic uncertainties, plus each experiment tends to be specific to the chosen setup and therefore difficult to generalize. Even if we used Direct Numerical Simulation (DNS), which we cannot do yet due to the high Reynolds number of the wind flow, resolving the blades correctly would still require an actuator-line model or similar parameterization, which would add some uncertainty.

Appendix A: Supplemental figures

Appendix A contains Figures A1 and A2 that were briefly discussed in the main text.

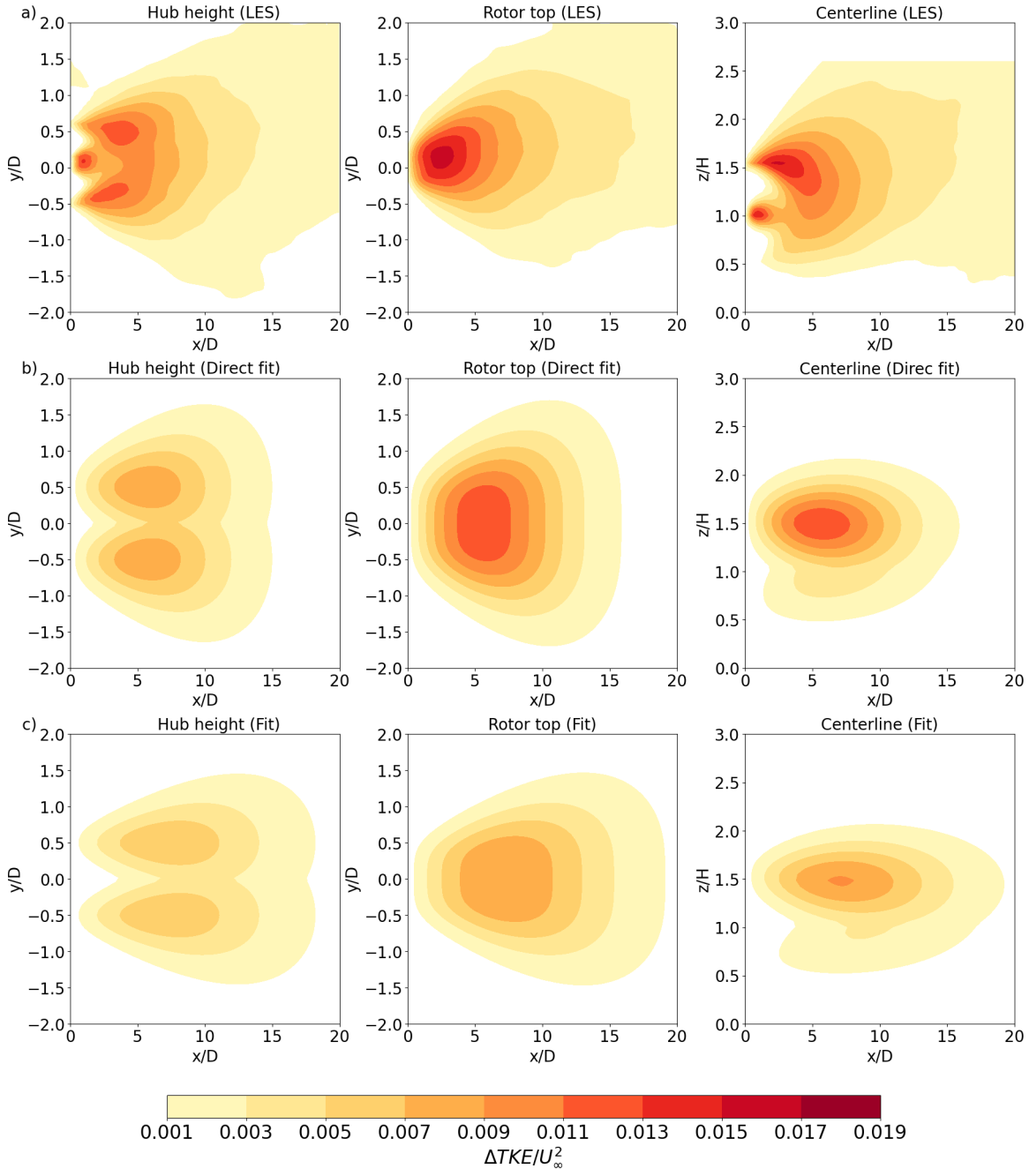

Figure A1. As in Fig. 3, but for unstable conditions (WRFLES-U).

Author contributions. Archer designed the research, obtained the funding, developed the formulation, and led the research; Khanjari led the Python coding and data processing; Archer and Khanjari analyzed the results and wrote the manuscript; Feroz helped with literature review and formulation development.

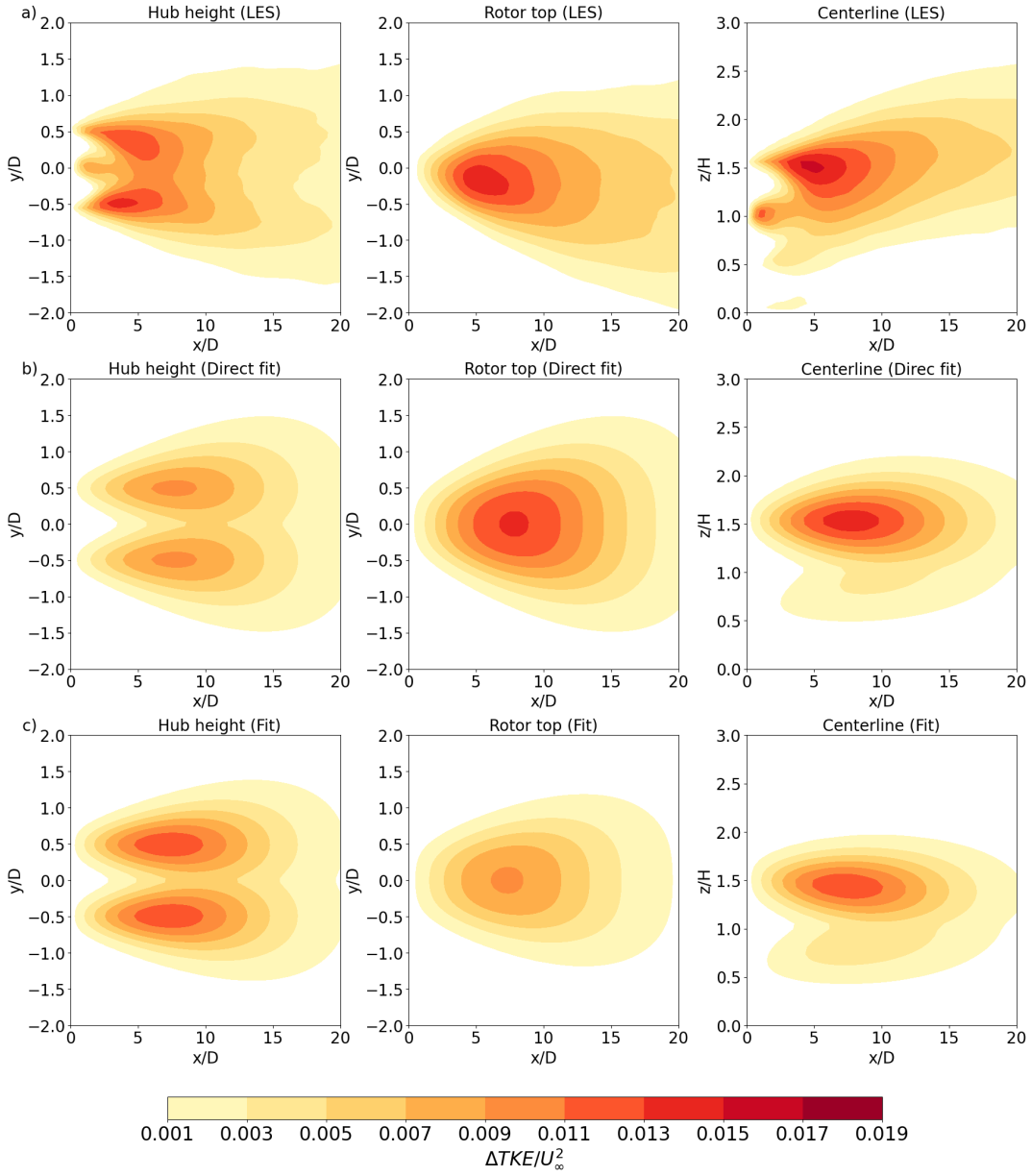

Figure A2. As in Fig. 3, but for stable conditions (WRFLES-S).

Competing interests. Archer is a member of the editorial board of Wind Energy Science.

Acknowledgements. Partial funding for this research was provided by a grant from First State Marine Wind. The authors are extremely thankful to Dr. Dara Vahidi and Fernando Porté-Agel at the Ecole Polytechnique Fédérale de Lausanne (EPFL, CH) for sharing their LES data and to Dr. Yaqing Jin and his team at University of Texas Dallas (USA) for sharing their wind tunnel data.

References

Abkar, M. and Porté-Agel, F.: A new wind-farm parameterization for large-scale atmospheric models, Journal of Renewable and Sustainable Energy, 7, 013 121, https://doi.org/doi: 10.1063/1.4907600, 2015.

Ainslie, J. F.: Calculating the flowfield in the wake of wind turbines, Journal of Wind Engineering and Industrial Aerodynamics, 27, 213–224, https://doi.org/10.1016/0167-6105(88)90037-2, 1988.

Aju, E. J., Suresh, D. B., and Jin, Y.: The influence of winglet pitching on the performance of a model wind turbine: Aerodynamic loads, rotating speed, and wake statistics, Energies, 13, https://doi.org/10.3390/en13195199, 2020.

Archer, C., Vasel-Be-Hagh, A., Yan, C., Wu, S., Pan, Y., Brodie, J., and Maguire, A.: Review and evaluation of wake loss models for wind energy applications, Applied Energy, 226, 1187–1207, https://doi.org/10.1016/j.apenergy.2018.05.085, 2018.

Archer, C. L. and Jacobson, M. Z.: Evaluation of global wind power, Journal of Geophysical Research – Atmospheres, 110, https://doi.org/10.1029/2004JD005462, 2005.

Archer, C. L., Mirzaeisefat, S., and Lee, S.: Quantifying the sensitivity of wind farm performance to array layout options using large-eddy simulation, Geophys Res Lett, 40, 4963–4970, https://doi.org/10.1002/grl.50911, 2013.

Archer, C. L., Wu, S., Vasel-Be-Hagh, A., Brodie, J. F., Delgado, R., Pé, A. S., Oncley, S., and Semmer, S.: The VERTEX field campaign: Observations of near-ground effects of wind turbine wakes, Journal of Turbulence, 20, 64–92, https://doi.org/10.1080/14685248.2019.1572161, 2019.

Archer, C. L., Wu, S., Ma, Y., and Jiménez, P.: Two corrections for the treatment of turbulent kinetic energy in the WRF model, Monthly Weather Review, 148, 4823—-4835, https://doi.org/10.1175/MWR-D-20-0097.1, 2020.

Arya, P.: Introduction to micrometeorology, Academic Press, 1988.

Arya, P.: Introduction to micrometeorology, 2nd Edition, Academic Press, 2001.

Barthelmie, R., Larsen, G., Pryor, S., Jørgensen, H., Bergström, H., Schlez, W., Rados, K., Lange, B., Vølund, P., Neckelmann, S., Mogensen, S., Schepers, G., Hegberg, T., Folkerts, L., and Magnusson, M.: ENDOW (Efficient Development of Offshore Wind Farms): Modelling wake and boundary layer interactions, Wind Energy, 7, 225–245, https://doi.org/10.1002/we.121, 2004.

Bastankhah, M. and Porté-Agel, F.: A new analytical model for wind-turbine wakes, Renewable Energy, 70, 116–123, https://doi.org/10.1016/j.renene.2014.01.002, 2014.

Bastankhah, M., Zunder, J. K., Hydon, P. E., Deebank, C., and Placidi, M.: Modelling turbulence in axisymmetric wakes: an application to wind turbine wakes, Journal of Fluid Mechanics, 1000, A2, https://doi.org/10.1017/jfm.2024.664, 2024.

Breton, S.-P., Sumner, J., Sørensen, J. N., Hansen, K. S., Sarmast, S., and Ivanell, S.: A survey of modelling methods for high-fidelity wind farm simulations using large eddy simulation, Philosophical Transactions of the Royal Society A: Mathematical, Physical and Engineering Sciences, 375, 20160 097, https://doi.org/10.1098/rsta.2016.0097, 2017.

Burton, T., Jenkins, N., Sharpe, D., and Bossanyi, E.: Wind energy handbook, John Wiley & Sons, 2011.

Cafiero, G., Obligado, M., and Vassilicos, J. C.: Length scales in turbulent free shear flows, Journal of Turbulence, 21, 243–257, 2020.

Churchfield, M., Lee, S., Moriarty, P., Martínez, L., Leonardi, S., Vijayakumar, G., and Brasseur, J.: Large-eddy simulations of wind-plant aerodynamics, pp. 1–19, 50th AIAA Aerospace Sciences Meeting, Nashville (Tennessee), 2012.

Crespo, A. and Hernández, J.: Turbulence characteristics in wind-turbine wakes, Journal of Wind Engineering and Industrial Aerodynamics, 61, 71–85, https://doi.org/10.1016/0167-6105(95)00033-X, 1996.

Crespo, A., Hernandez, J., and Frandsen, S.: Survey of modelling methods for wind turbine wakes and wind farms, Wind Energy, 2, 1–24, https://doi.org/10.1002/(SICI)1099-1824(199901/03)2:1<1::AID-WE16>3.0.CO;2-7, 1999.

Delvaux, T., van der Laan, M. P., and Terrapon, V. E.: A new RANS-based added turbulence intensity model for wind-farm flow modelling, Journal of Physics: Conference Series, 2767, 092 089, https://doi.org/10.1088/1742-6596/2767/9/092089, 2024.

Deskos, G., Laizet, S., and Piggott, M. D.: Turbulence-resolving simulations of wind turbine wakes, Renewable Energy, 134, 989–1002, https://doi.org/10.1016/j.renene.2018.11.084, 2019.

Eriksson, O., Lindvall, J., Breton, S.-P., and Ivanell, S.: Wake downstream of the Lillgrund wind farm - A Comparison between LES using the actuator disc method and a wind farm parametrization in WRF, Journal of Physics: Conference Series, 625, 012 028, https://doi.org/10.1088/1742-6596/625/1/012028, 2015.

Feng, D., Li, L. K., Gupta, V., and Wan, M.: Componentwise influence of upstream turbulence on the far-wake dynamics of wind turbines, Renewable Energy, 200, 1081–1091, https://doi.org/10.1016/j.renene.2022.10.024, 2022.

Fischereit, J., Brown, R., Larsén, X. G., Badger, J., and Hawkes, G.: Review of mesoscale wind-farm parametrizations and their applications, Boundary-Layer Meteorology, 182, 175—224, https://doi.org/10.1007/s10546-021-00652-y, 2022.

Fitch, A. C., Olson, J. B., Lundquist, J. K., Dudhia, J., Gupta, A. K., Michalakes, J., and Barstad, I.: Local and mesoscale impacts of wind farms as parameterized in a mesoscale NWP model, Monthly Weather Review, 140, 3017 – 3038, https://doi.org/10.1175/MWR-D-11-00352.1, 2012.

Frandsen, S., Barthelmie, R., Pryor, S., Rathmann, O., Larsen, S., Højstrup, J., and Thøgersen, M.: Analytical modelling of wind speed deficit in large offshore wind farms, Wind Energy, 9, 39–53, https://doi.org/10.1002/we.189, 2006.

Gao, X., Yang, H., and Lu, L.: Optimization of wind turbine layout position in a wind farm using a newly-developed two-dimensional wake model, Applied Energy, 174, 192–200, https://doi.org/10.1016/j.apenergy.2016.04.098, 2016.

Ghaisas, N. S., Archer, C. L., Xie, S., Wu, S., and Maguire, E.: Evaluation of layout and atmospheric stability effects in wind farms using large-eddy simulation, Wind Energy, 20, 1227–1240, https://doi.org/10.1002/we.2091, 2017.

Göçmen, T., Van der Laan, P., Réthoré, P.-E., Diaz, A. P., Larsen, G. C., and Ott, S.: Wind turbine wake models developed at the Technical University of Denmark: A review, Renewable and Sustainable Energy Reviews, 60, 752–769, https://doi.org/10.1016/j.rser.2016.01.113, 2016.

Hassan, U.: A wind tunnel investigation of the wake structure within small wind turbine farms, Tech. Rep. ETSU-WN-5113, Department of Energy, United Kingdom, 1993.

International Electrotechnical Commission: Wind energy generation systems - Part 1: Design requirements, Tech. Rep. IEC 61400-1 Ed. 4.0 B:2019, IEC, Denmark, https://webstore.ansi.org/standards/iec/iec61400ed2019-2419167?source=blog, 2019.

International Renewable Energy Agency (IRENA): Wind Energy, https://www.irena.org/Energy-Transition/Technology/Wind-energy, accessed: 2023-10-23, 2022.

Ishihara, T. and Qian, G.-W.: A new Gaussian-based analytical wake model for wind turbines considering ambient turbulence intensities and thrust coefficient effects, Journal of Wind Engineering and Industrial Aerodynamics, 177, 275–292, https://doi.org/10.1016/j.jweia.2018.04.010, 2018.

Jensen, N. O.: A note on wind generator interaction, Tech. Rep. Risø-M-2411, Risø National Laboratory, Denmark, 1983.

Johansson, P. B., George, W. K., and Gourlay, M. J.: Equilibrium similarity, effects of initial conditions and local Reynolds number on the axisymmetric wake, Physics of Fluids, 15, 603–617, 2003.

Katic, I., Højstrup, J., and Jensen, N. O.: A simple model for cluster efficiency, pp. 407–410, European Wind Energy Association Conference and Exhibition (EWEC'86), Rome, 1986.

Kim, J. and Moin, P.: Application of a fractional-step method to incompressible Navier-Stokes equations, Journal of Computational Physics, 59, 308–323, https://doi.org/10.1016/0021-9991(85)90148-2, 1985.

Larsen, G. C.: A simple wake calculation procedure, Tech. Rep. Risø-M-2760, Risø National Laboratory, Denmark, 1988.

Larsén, X. G.: Calculating Turbulence Intensity from mesoscale modeled Turbulence Kinetic Energy, Tech. Rep. E-0233, Danish Technical Univerity Wind Energy, Denmark, https://backend.orbit.dtu.dk/ws/portalfiles/portal/364980906/TKE2TI-20240627.pdf, 2022.

Lee, J. C. and Lundquist, J. K.: Observing and simulating wind-turbine wakes during the evening transition, Boundary-Layer Meteorology, 164, 449–474, https://doi.org/10.1007/s10546-017-0257-y, 2017.

Li, L., Huang, Z., Ge, M., and Zhang, Q.: A novel three-dimensional analytical model of the added streamwise turbulence intensity for wind-turbine wakes, Energy, 238, 121 806, https://doi.org/10.1016/j.energy.2021.121806, 2022.

Lissaman, P. B. S.: Energy effectiveness of arbitrary arrays of wind turbines, Journal of Energy, 3, 323–328, https://doi.org/10.2514/3.62441, 1979.

Ma, Y., Archer, C. L., and Vasel-Be-Hagh, A.: Comparison of individual versus ensemble wind farm parameterizations inclusive of sub-grid wakes for the WRF model, Wind Energy, 25, 1573–1595, https://doi.org/10.1002/we.2758, 2022a.

Ma, Y., Archer, C. L., and Vasel-Be-Hagh, A.: The Jensen wind farm parameterization, Wind Energy Science, 7, 2407–2431, https://doi.org/10.5194/wes-7-2407-2022, 2022b.

Madsen, H. A.: A CFD analysis of the actuator disc flow compared with momentum theory results, in: Proceedings of the 10th Symposium on Aerodynamics of Wind Turbines, pp. 109–124, IEA Joint Action, 1996.

Martínez-Tossas, L. A., Churchfield, M. J., and Meneveau, C.: Optimal smoothing length scale for actuator line models of wind turbine blades based on Gaussian body force distribution, Wind Energy, 20, 1083–1096, https://doi.org/10.1002/we.2081, 2017.

Meyers, J. and Meneveau, C.: Large-eddy simulations of large wind-turbine arrays in the atmospheric boundary layer, 48th AIAA Aerospace Sciences Meeting Including the New Horizons Forum and Aerospace Exposition, Orlando, FL, https://doi.org/10.2514/6.2010-827, 2010.

Mikkelsen, R. F.: Actuator disc methods applied to wind turbines, Phd thesis, Technical University of Denmark, (DTU), mEK-FM-PHD No. 2003-02, 2003.

Mirocha, J. D., Kosovic, B., Aitken, M. L., and Lundquist, J. K.: Implementation of a generalized actuator disk wind turbine model into the Weather Research and Forecasting model for large-eddy simulation applications, Journal of Renewable and Sustainable Energy, 6, 013 104, https://doi.org/10.1063/1.4861061, 2014.

Moeng, C., Dudhia, J., Klemp, J., and Sullivan, P.: Examining two-way grid nesting for large eddy simulation of the PBL using the WRF model, Mon. Weather Rev., 135, 2295–2311, https://doi.org/10.1175/MWR3406.1, 2007.

Nygaard, N. G.: Wakes in very large wind farms and the effect of neighbouring wind farms, Journal of Physics: Conference Series, 524, 012 162, https://doi.org/10.1088/1742-6596/524/1/012162, 2014.

Pan, Y. and Archer, C. L.: A hybrid wind-farm parametrization for mesoscale and climate models, Boundary-Layer Meteorology, 168, 469–495, https://doi.org/10.1007/s10546-018-0351-9, 2018.

Quarton, D. and Ainslie, J.: Turbulence in wind turbine wakes, Wind Engineering, 14, 15–23, 1990.

Santoni, C., Carrasquillo, K., Arenas-Navarro, I., and Leonardi, S.: Effect of tower and nacelle on the flow past a wind turbine, Wind Energy, 20, 1927–1939, https://doi.org/10.1002/we.2130, 2017.

Sherry, M., Nemes, A., Lo Jacono, D., Blackburn, H. M., and Sheridan, J.: The interaction of helical tip and root vortices in a wind turbine wake, Physics of Fluids, 25, 117 102, https://doi.org/10.1063/1.4824734, 2013.

Siedersleben, S., Platis, A., Lundquist, J., Djath, B., Lampert, A., Bärfuss, K., Cañadillas, B., Schulz-Stellenfleth, J., Bange, J., Neumann, T., and Emeis, S.: Turbulent kinetic energy over large offshore wind farms observed and simulated by the mesoscale model WRF (3.8.1), Geoscientific Model Development, 13, 249–268, https://doi.org/10.5194/gmd-13-249-2020, 2020.

Skamarock, W. C., Klemp, J. B., Dudhia, J., Gill, D. O., Liu, Z., Berner, J., Wang, W., Powers, J. G., Duda, M. G., Barker, D., and Huang, X.-y.: A description of the Advanced Research WRF Model Version 4.3, Tech. rep., National Center for Atmospheric Research, Boulder, Colorado, USA, https://doi.org/10.5065/1dfh-6p97, no. NCAR/TN-556+STR, 2021.

Sørensen, J. N. and Myken, A.: Unsteady actuator disc model for horizontal axis wind turbines, Journal of Wind Engineering and Industrial Aerodynamics, 39, 139–149, 1992.

Sorensen, J. N. and Shen, W. Z.: Numerical modeling of wind turbine wakes, J. Fluids Eng., 124, 393–399, 2002.

Stevens, R. J. and Meneveau, C.: Flow structure and turbulence in wind farms, Annual Review of Fluid Mechanics, 49, 311–339, https://doi.org/10.1146/annurev-fluid-010816-060206, 2017.

Stull, R.: Practical meteorology: An algebra-based survey of atmospheric science, University of British Columbia, https://www.eoas.ubc.ca/books/Practical_Meteorology/, 2017.

Tian, L., Song, Y., Xiao, P., Zhao, N., Shen, W., and Zhu, C.: A new three-dimensional analytical model for wind turbine wake turbulence intensity predictions, Renewable Energy, 189, 762–776, https://doi.org/10.1016/j.renene.2022.02.115, 2022.

Vahidi, D. and Porté-Agel, F.: Influence of thrust coefficient on the wake of a wind turbine: A numerical and analytical study, Renewable Energy, 240, 122 194, https://doi.org/10.1016/j.renene.2024.122194, 2025.

van der Laan, M. P., Baungaard, M., and Kelly, M.: Brief communication: A clarification of wake recovery mechanisms, Wind Energy Science, 8, 247–254, https://doi.org/10.5194/wes-8-247-2023, 2023.

Vanderwende, B. J., Kosović, B., Lundquist, J. K., and Mirocha, J. D.: Simulating effects of a wind-turbine array using LES and RANS, Journal of Advances in Modeling Earth Systems, 8, 1376–1390, https://doi.org/10.1002/2016MS000652, 2016.

Vermeer, L., Sørensen, J. N., and Crespo, A.: Wind turbine wake aerodynamics, Progress in Aerospace Sciences, 39, 467–510, https://doi.org/10.1016/S0376-0421(03)00078-2, 2003.

Wang, T., Cai, C., Wang, X., Wang, Z., Chen, Y., Song, J., Xu, J., Zhang, Y., and Li, Q.: A new Gaussian analytical wake model validated by wind tunnel experiment and LiDAR field measurements under different turbulent flow, Energy, 271, 127 089, https://doi.org/https://doi.org/10.1016/j.energy.2023.127089, 2023.

Wilcox, D.: Turbulence modeling for CFD, 3rd Edition, Birmingham Press, Inc., San Diego, California, USA, 2006.

Wu, S. and Archer, C. L.: Near-ground effects of wind turbines: Observations and physical mechanisms, Monthly Weather Review, 149, 879 – 898, https://doi.org/10.1175/MWR-D-20-0186.1, 2021.

Wu, S., Archer, C. L., and Mirocha, J.: New insights on wind turbine wakes from large-eddy simulation: Wake contraction, dual nature, and temperature effects, Wind Energy, pp. 1–22, https://doi.org/10.1002/we.2827, 2023.

Xie, S. and Archer, C.: Self-similarity and turbulence characteristics of wind turbine wakes via large-eddy simulation, Wind Energy, 18, 1815–1838, https://doi.org/10.1002/we.1792, 2015.

Xie, S. and Archer, C. L.: A numerical study of wind-turbine wakes for three atmospheric stability conditions, Boundary-Layer Meteorol, 165, 87–112, https://doi.org/10.1007/s10546-017-0259-9, 2017.

Yang, X., Howard, K. B., Guala, M., and Sotiropoulos, F.: Effects of a three-dimensional hill on the wake characteristics of a model wind turbine, Physics of Fluids, 27, 025 103, https://doi.org/10.1063/1.4907685, 2015.

Ye, M., Chen, H.-C., and Koop, A.: High-fidelity CFD simulations for the wake characteristics of the NTNU BT1 wind turbine, Energy, 265, 126 285, https://doi.org/10.1016/j.energy.2022.126285, 2023.